Direct Air Capture of CO_2 Using Amino Acid Solutions and Porous Catalysts

A Thesis

SUBMITTED TO THE FACULTY OF THE

UNIVERSITY OF MINNESOTA

BY

Olajumobi Rachael Akeeb

IN PARTIAL FUFILLMENT OF THE REQUIREMENTS

FOR THE DEGREE OF

MASTER OF SCIENCE

Advisor: Dr. Sam Toan, Supervisor: Dr. Lei Wang

May 2022

Acknowledgements

I would like to express my gratitude to my advisor, Dr. Sam Toan, who guided me throughout this project. Your patience and expertise was invaluable in completing this research. I would also like to thank my supervisor Dr. Lei Wang, your insightful feedback and collaboration brought my work to a higher level. In addition, the help provided by the faculty and staff in the Chemical Engineering department at the University of Minnesota Duluth provided me with the tools I needed to successfully complete my research. And finally I would like to thank my friends and family who supported me and offered a great deal of support throughout the research and writing process.

Abstract

Increasing CO_2 in the atmosphere has led to an increase in global climate change, and this already has an observable effect on the environment. In recent years, there have been accelerated sea level rise, intense heat waves, loss of sea ice, plants flowering sooner, shrinking glaciers among other adverse effects. CO_2 capture has the potential to reduce CO_2 emissions from new and existing coal- and gas- fired power plants, industrial processes, and other sources of CO_2. Aqueous monoethanolamine (MEA) mixtures for carbon capture have been widely popular for decades, due to their low cost, high absorption capacity and low regeneration heat requirement. However, they are also extremely volatile, they degrade in oxygen rich environments, and form degradation products that are toxic to human health and the environment. Recently, amino acids have emerged as an alternative to the use of monoethanolamine for CO_2 capture. This is because of their stability, low toxicity, moderate capture performance, and that they are a naturally occurring substance.

This research focuses on the capture performance of eight systems in comparison to MEA. Including, L-arginine, L-histidine, L-lysine, Glycine, L-arginine salt, L-histidine salt, L-lysine salt, and Glycine salt solutions. Attention is given to the cumulative absorption, cumulative desorption, desorption rate and breakthrough times of each system. The concentration of each solution studied is 10 mmol or 0.25 M, with the experiments occurring at atmospheric pressure 1 atm. The apparatus used in the experiment obtained data at room temperature (20 – 25 ºC) during absorption and 70 –

95 °C during desorption. It was found that a number of amino acid and amino acid salt solutions tested could replace MEA, however the solutions of L-lysine and L-lysine salt showed the most promise.

This thesis includes a brief introduction to the central issues of this work, explaining the relevance with global climate change in perspective. Then carbon management technologies are discussed, including the limits of the current technologies and the possibilities available with direct air capture using amino acids. Excerpts from a previously published review paper on post-combustion CO_2 capture is included to provide more context for this work. The experimental process is also explained in detail, including absorbent selection, catalyst selection, absorbent and catalyst preparation, the experimental procedure and catalyst characterization. Finally, the results of the experiments are discussed, followed by the accomplishments of this project and future work.

Table of Contents

List of Tables

List of Figures

List of Abbreviations

Abbreviations	Definition
3DG	3D-Graphene
BET	Brunauer-Emmett-Teller
CCS	Carbon Capture And Storage
CCU	Carbon Capture And Utilization
CH_4	Methane
CO_2	Carbon Dioxide
COOH	Carboxyl Group
DAC	Direct Air Capture
DI	Deionized
EDS	Energy-Dispersive X-Ray Spectrometry
EPA	Environmental Protection Agency
FESEM	Field Emission Scanning Electron Microscope
GHG	Greenhouse Gases
H_2	Hydrogen
IEA	International Energy Agency
IEAGHG	IEA Greenhouse Gas R&D Program
IGCC	Integrated Gasification Combined Cycle
K_2CO_3	Potassium Carbonate
KOH	Potassium Hydroxide
MEA	Monoethanolamine
MFC	Mass Flow Controller
N2	Nitrogen
N_2O	Nitrous Oxide
NASA	National Aeronautics And Space Administration
NETL	National Energy Technology Laboratory
NO_X	Nitrogen Oxides
OH	Hydroxide
SBA-15	Santa Barbara Amorphous-15
SEM	Scanning Electron Microscope
SSA	Specific Surface Area
TEM	Transmission Electron Microscope
XPS	X-Ray Photoelectron Spectroscopy
XRD	X-Ray Diffraction

Chapter 1: Introduction

Direct air capture (DAC) technology is one of the few options available and currently researched method for the removal of carbon dioxide (CO_2) from the atmosphere. DAC involves the process of capturing CO_2 from air, with a goal to offset emission from fossil fuels.

1.1. Climate Change

Increasing CO_2 in the atmosphere is leading to an increase in global climate change. This already has an observable effect on the environment (NASA 2022). Effects that scientists had predicted in the past, resulting from global climate change are now occurring: accelerated sea level rise, intense heat waves, loss of sea ice, plants flowering sooner, shrinking glaciers (NASA 2022).

Since the age of industrialization, the concentration of greenhouse gases (GHG) in the atmosphere has been on the rise. Human activities especially the burning of fossil fuels has greatly contributed to this increase. GHGs trap heat in the atmosphere, making the planet warmer and 'thickening the Earth's blanket' (EPA 2022). The four GHGs produced from the process of burning fossil fuels include: carbon dioxide (CO_2), methane (CH_4), nitrous oxide (N_2O), and fluorinated gases (hydrofluorocarbons, perfluorocarbons, sulfur hexafluoride, and nitrogen trifluoride) (EPA 2022). These gases can stay in the atmosphere for a period of time ranging from a few years to thousands of years, and they remain in the atmosphere long enough to become well mixed, meaning that the amount that is measured in the atmosphere is roughly the same

all over the world, regardless of the source of the emissions (EPA 2022). Figure 1 below shows the overview of U.S. GHG emissions in 2020, with CO_2 alone totaling 5,981 million metric tons or 79% of GHGs (EPA 2022).

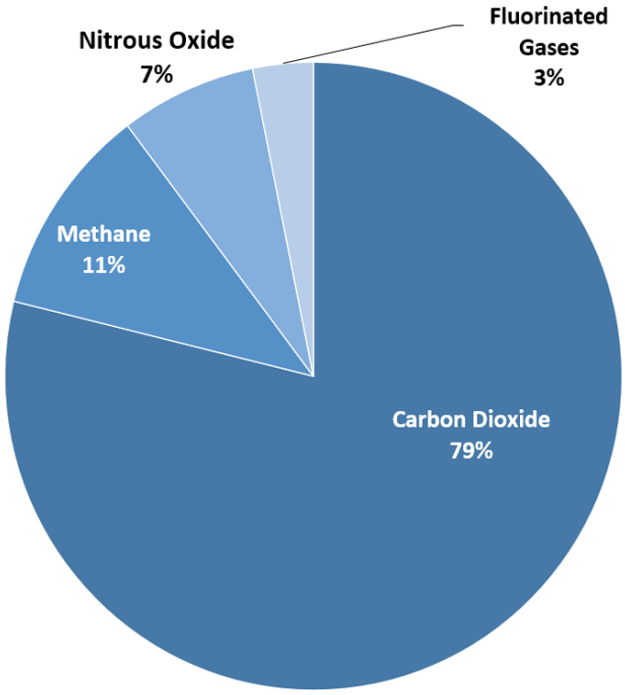

U.S. Environmental Protection Agency (2022). Inventory of U.S. Greenhouse Gas Emissions and Sinks: 1990-2020

Figure 1. Overview of U.S. Greenhouse Gas Emissions in 2020 (EPA 2022).

1.2. Sources of CO_2 in the atmosphere

CO_2 is the primary GHG emitted through human activities, and in 2020 alone CO_2 accounted for about 79% of all U.S. GHG emissions from human activities as show in Figure 1 above. CO_2 is naturally present in the atmosphere as part of the Earth's carbon cycle, but human activities have altered, and are continuing to alter the carbon cycle. Both by adding more CO_2 to the atmosphere and by influencing the ability of natural sinks, like forests and soils, to remove and store CO_2 from the atmosphere (EPA 2022). According to NASA, CO_2 concentration is currently at its highest level in

650,000 years, at 417 ppm, the global temperature has also risen 1.01 ºC since 1880 (NASA 2022). Figure 2 and Figure 3 below show the increase of CO_2 concentration over time and the increase of global temperature over time respectively.

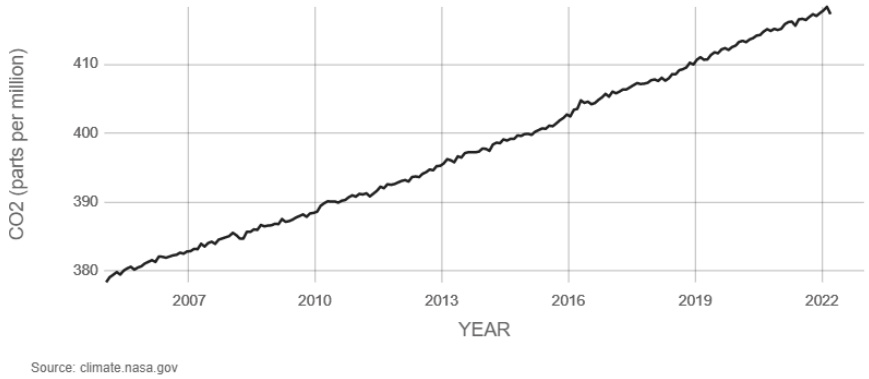

Figure 2. Monthly Measurements of Carbon Dioxide 2005-Present (NASA 2022).

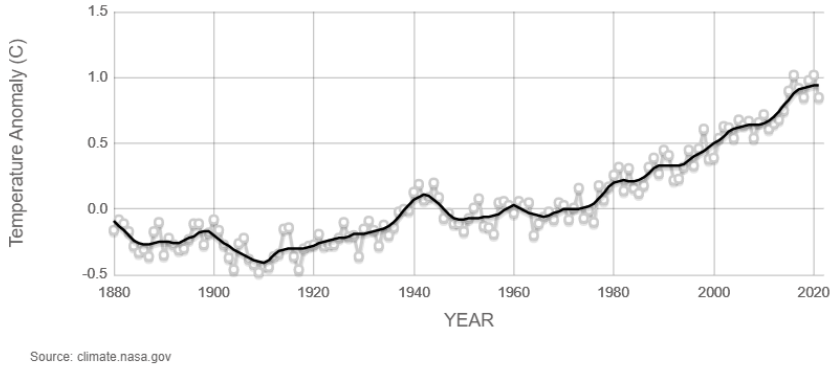

Figure 3. Global Temperature Index 1880-2020 (NASA 2022).

The primary human activity that emits CO_2 is the combustion of fossil fuels (coal, natural gas, and oil) for energy and transportation, although certain industrial processes and land-use changes also emit CO_2 (EPA 2022). In the Unites States (U.S.), transportation accounted for 33% of the total CO_2 emissions in 2020, from the combustion of fossil fuels such as gasoline and diesel. In the same year, electricity accounted for 31% of CO_2 emissions, followed by industrial processes at 16%,

residential and commercial use of fossil fuels at 12% and other non-fossil fuel combustion processes at 8% (EPA 2022). All of this is summarized in Figure 4 below.

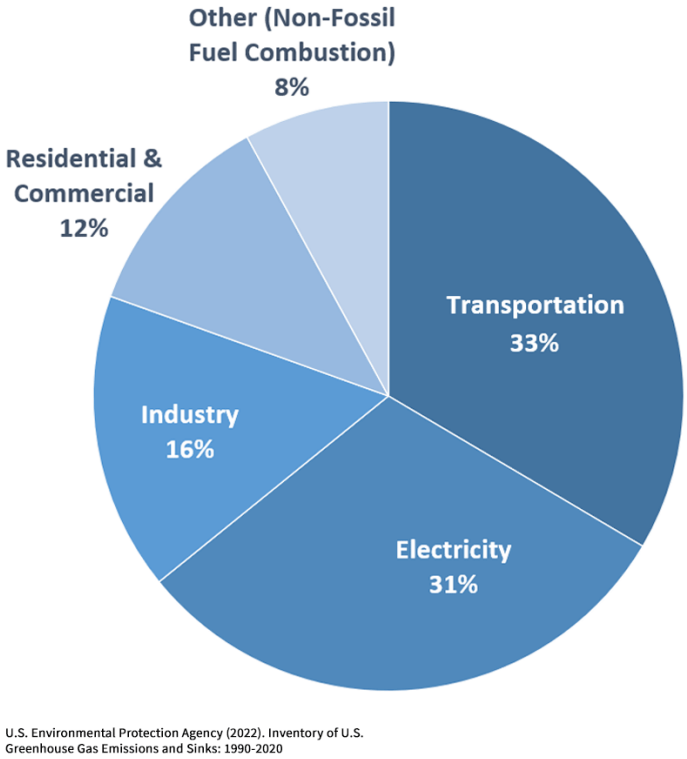

Figure 4. 2020 U.S. Carbon Dioxide Emissions, By Source (EPA 2022).

1.3. Carbon management technologies

Research into the technologies that can be used to mitigate the increasing concentration of CO_2 in the atmosphere has been driven forward by global concerns over climate change. Carbon management technologies aim to manage anthropogenic releases of GHGs associated with the combustion of fossil fuels, in an effort to mitigate the potential impacts of these emissions on climate systems (Paul J. Runci 2004). There are different approaches that can be taken in an effort to reduce CO_2 emissions, including energy efficiency, fuel switching, combined heat and power, use of renewable energy, more efficient use and recycling of materials, etc. However, industrial process do not

have existing low-emission alternatives, leading to a requirement of carbon capture and storage to reduce emission long term (C2ES).

1.4. Carbon capture and storage/utilization

Carbon capture and storage or sequestration (CCS) is a set of technologies that can potentially greatly reduce CO_2 emissions from new and existing coal- and gas- fired power plants, industrial processes, and other stationary sources of CO_2 (EPA 2022). It is a technological process removes CO_2 from emission streams, transports it and permanently and safely stores it underground at a carefully selected and suitable subsurface geologic formation (EPA 2022, WRI 2022).

Carbon capture and utilization (CCU) on the other hand is a process that captures CO_2 emissions from sources like coal-fired power plants mentioned above and reuses it (DOE). The CCU process converts the captured CO_2 into more valuable products like: plastics, concrete, and biofuel, with a goal of net zero CO_2 emissions.

Carbon capture can be classified into three categories: oxy-fuel combustion, pre-combustion, and post-combustion. The three technologies are discussed in detail in Chapter 2.

1.5. Limits on conventional technologies

Carbon capture via absorption through aqueous amine solutions is one of the most widely implemented technologies for post-combustion capture. It has been widely used to remove CO_2 in industrial applications for decades (Sorensen 2016). The process involves aqueous amine solutions absorbing acidic gases, including CO_2 which then forms carbonic acid in water (Sorensen 2016). After absorption, the solution is heated

in order to release the captured gases for further reaction or into containment for storage. Aqueous monoethanolamine (MEA) mixtures are the leading absorbents for post-combustion CO_2 capture. The low cost, high absorption capacity, and low regeneration heat requirement makes it a very attractive process (Olajumobi Akeeb 2022). However there is a high energy requirement because of the high heat of reaction for CO_2 and MEA (Olajumobi Akeeb 2022).

For example, when burning coal, the theoretical minimum energy to extract CO_2 from the flue gas and pressurize it for efficient storage (150 bar) is 396k J/kg of CO_2, although the lowest energy claimed to be achievable is closer to 720 kJ/kg (Rochelle 2009). And given that typical coal consumption yield is 3.65 MJ/kg CO_2, this means carbon sequestration for coal would require at least 10 % of the produced energy to be diverted to the sequestration process, and in reality would divert 20 % or more, making carbon sequestration an expensive proposition (Krey V. 2014). This calculation ignores the energy costs of pumping the CO_2 to the storage point, which could raise costs substantially for sufficiently remote storage locations (Sorensen 2016). Furthermore, as CO_2 cannot be fully absorbed into the amine solution, the process can, at most, absorb 85-90 % of the emitted CO_2 (Sorensen 2016). And assuming extra coal is burned to compensate for the energy cost of sequestration, this would mean that CO_2 emissions from these power plants would remain at at-least 12.5-18.75 % of original levels should all coal plants be fitted with these technologies, and likely higher assuming not all plants were able to achieve the lowest-level 20 % energy consumption (Sorensen 2016). So while this carbon capture technology could reduce CO_2 emissions from coal use in

particular, it would also make coal-based energy expensive and uncompetitive in the economy.

1.6. Direct air capture (DAC) of CO_2

As previously mentioned above in section 1. , direct air capture (DAC) technology is one of the available options for CO_2 capture from the atmosphere. According to the IEA, some benefits of DAC as a carbon removal option include its limited land and water footprint and the viability of locating plants on non-arable land close to suitable storage, eliminating the need for long-distance CO_2 transport (IEA 2021). Although the implementation of DAC is currently possible, several issues make its general implementation difficult. Constraints like costs and energy requirements as well as the potential for pollution makes it a less desirable option for CO_2 capture (Rhode, 2021). Its larger land footprint when compared to other mitigation also puts it at a disadvantage. The CO_2 in the atmosphere is far more dilute than CO_2 in flue gas for example, and this adds to the energy need and coast for DAC, relative to other technologies. According to the IEA, costs and energy needs vary according to the type of technology and whether the captured CO_2 is going to be geologically stored or used immediately at low pressure (IEA 2021). In reality, CO_2 needs to be compressed under very high pressure for it to be injected into geological formations. This step increases both the plant's capital costs (due to the requirement for additional equipment such as a compressor) and operating expenses (to run the compressor) (IEA 2021). Figure 5 below summarizes the energy needs by technology and CO_2 destination.

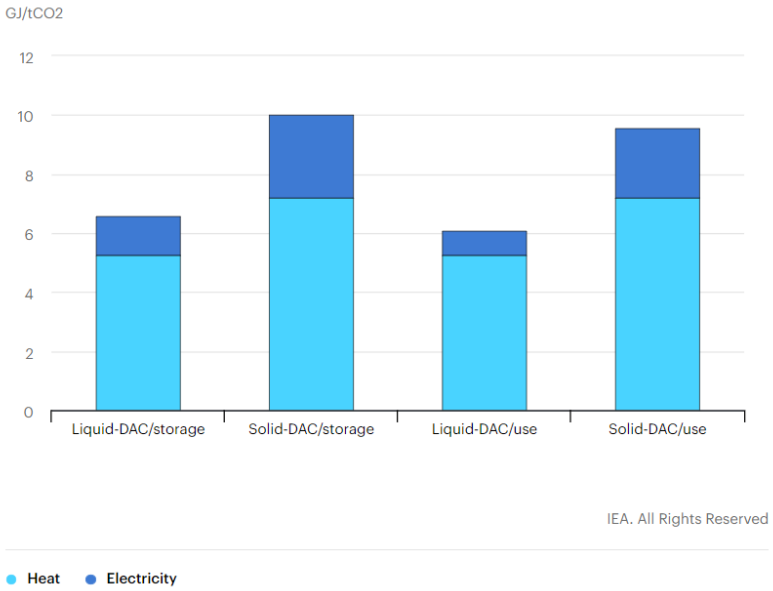

Figure 5. DAC Energy Needs By Technology and CO_2 Destination (large-scale applications), 2021 (IEA 2021).

DAC technology has yet to be demonstrated as a large scale process, so its future cost is uncertain (IEA 2021). Capture cost estimates are wide-ranging, from USD 100/t to USD 1 000/t (IEA 2021). Although in 2018, Carbon Engineering released peer-reviewed research showing that capture costs of USD 94/t to USD 232/t were achievable depending on financial assumptions, energy costs and specific plant configuration (IEA 2021). Nineteen DAC plants are currently operational in Europe, the United States and Canada, but most of these plants are small and sell the captured CO_2 for use; for carbonating drinks, for example. The first large-scale DAC plant is now being developed in the United States through a Carbon Engineering and Occidental Petroleum partnership. The plant will capture up to 1 Mt CO_2 each year and could become operational as early as 2024 (IEA 2021). Amino acid salt systems are currently gaining much attention in the research for CO_2 capture technologies. This thesis studies both amino acids and amino acid salts for CO_2 capture.

1.7. Goal and hypotheses

CO_2 capture from air seems to be a promising and fairly well researched technology. Although it qualifies as a novel/conventional technology with various systems being developed, it has yet to be demonstrated beyond lab-, and small- scale processes. The research also focuses on MEA sorbent systems which have high energy requirements and are not environmentally friendly. MEA sorbents can degrade in nitrosamines, which can be emitted during the capture process into the environment. Human health hazards have been associated with degradation products like that, including potential long-term effects associated with mutagenicity, genotoxicity/carcinogenicity, and reproduction (Andy Bootha 2011). Absorbing CO_2 from the atmosphere while also using technology that negatively impacts the people and environment is not the best long-term solution.

The aim of this thesis is to explore other absorption systems like amino acid and amino acid salt solutions. Amino acids have attracted special attention recently because of their low volatility, low toxicity, and capture performance when compared to conventional amines (Ramezani, Mazinani et al. 2022). In this study, four different amino acid and amino acid salt solutions are tested for CO_2 absorption and desorption. Their performance as standalone solutions are discussed and compared to MEA, then the best amino acid solution is studied with different catalysts in order to improve its performance.

The goals are as follows:

(i) Conduct CO_2 capture experiments with various amino acid systems

(ii) Determine most viable system from the experiments, and improve capture

capacity and breakthrough time via the implementation of catalysts

(iii) Prove the stability of the chosen system for future applications

This project is based on the following hypotheses:

Hypothesis 1: Amino acid solutions have the potential to replace MEA for CO_2 capture

Hypothesis 2: Amino acids have moderate capture capacity, are more stable, and less volatile than MEA

Hypothesis 3: The use of porous catalysts can improve the capture capacity and breakthrough time of amino acid solutions

Chapter 2: Excerpts from previous research paper*

Post-combustion CO_2 capture via a variety of temperature ranges and material adsorption process: A Review

It has been repeatedly demonstrated that increasing GHG concentration in the atmosphere contributes to increased air pollution, extreme weather, food supply disruptions, and increased wildfires. GHG emissions from fossil fuel combustion must be minimized to avoid biodiversity destruction, ocean acidification, and myriad other environmental impacts. Carbon capture and storage/sequestration (CCS) were first implemented in the 1920s to separate CO_2 from methane extracted from natural gas reservoirs. CCS was first suggested for reducing anthropogenic CO_2 emissions in 1977 (IEAGHG 2017).

Chemical absorption (e.g., using aqueous amine solutions) has been utilized in two commercial-scale post-combustion capture facilities in coal-fired power plants: Boundary Dam and Petra Nova (Bui, Adjiman et al. 2018).

Despite the pressing need to commercialize CCS technologies, their large-scale deployment has been slow. As of November 2019, the USA has more than half of the global large-scale CCS facilities (Beck 2019). CCS technologies can be classified into

* The material contained in this chapter was previously published in the Journal of Environmental Management, Elsevier 2022, 313(1), 115026. https://doi.org/10.1016/j.jenvman.2022.115026. by Olajumobi Akeeb, Lei Wang, Weiguo Xie, Richard Davis, Malek Alkasrawi, Sam Toan.

the three categories described in Figure 6: oxy-fuel combustion, pre-combustion, and post-combustion (Herzog, Meldon et al. 2009).

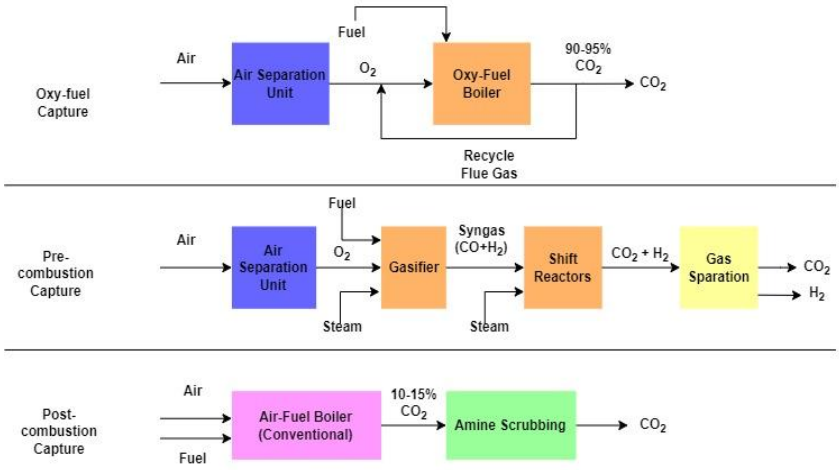

Figure 6. CO2 Capture Technologies By Category (Tara 2021).

Oxy-fuel combustion capture uses high purity oxygen for combusting coal with high CO_2 effluent concentration. Oxygen, the costliest component, is produced on-site via air separation (Herzog, Meldon et al. 2009). The oxygen can be diluted with a portion of the flue gas instead of nitrogen or air to control the temperature of the capture process. Although oxy-fuel combustion capture has some advantages, including reduced NO_X emissions and high CO_2 purity with lower gas volumes due to increased density, the process has a high energy demand for producing high purity oxygen (Carpenter and Long 2017). It generates substantial heat due to the combustion in a pure oxygen environment, which requires the flue gas to be recycled in large quantities to keep temperatures at reasonable levels (Adams 2014).

Pre-combustion capture refers to the separation of CO_2 before the combustion of another fuel, typically hydrogen. According to Rackley, it involves decarbonation by gasification of the primary fuel, commonly coal or biomass, through a combination of

partial combustion, steam reforming, water-gas shifting, and the separation of CO_2 from the resulting reaction product stream. It is most commonly affiliated with integrated coal-gasification combined-cycle (IGCC) plants, where coal is first gasified to form synthesis gas (or syngas, a mixture mainly comprised of carbon monoxide (CO) and hydrogen (H_2)) (Rackley 2017).

During the gasification process, coal is converted to gas using a gasifying agent (air, steam, or oxygen) (Abanades, Alonso et al. 2011, Heidenreich, Müller et al. 2016). The syngas then undergoes the water-gas shift reaction of CO with steam to form CO_2 and additional H_2. The CO_2 is then captured, and the H_2 is diluted with air and fed into a gas turbine combined cycle. Although pre-combustion capture has a cost advantage over post-combustion capture processes, there are only a few IGCC plants in the existing coal fleet because it costs too much to produce hydrogen, thus less prevalent than pulverized coal (PC) or natural gas power plants, where hydrocarbons are directly combusted to form CO_2 (Herzog, Meldon et al. 2009).

Post-combustion capture removes CO_2 from the flue gas after burning the fossil fuel. At present, all conventional coal-fired power plants combust primary coals directly to generate power (Merkel, Lin et al. 2010). Thus post-combustion capture is a more viable choice for existing coal-fired power plants as an "end-of-pipe" technology. Several post-combustion methods are used to capture CO_2, including adsorption (Harlick and Tezel 2003), membrane separation (Zhao, Riensche et al. 2008), or absorption (Rochelle 2009). Figure 7 represents a summary of post-combustion CO_2 capture technologies.

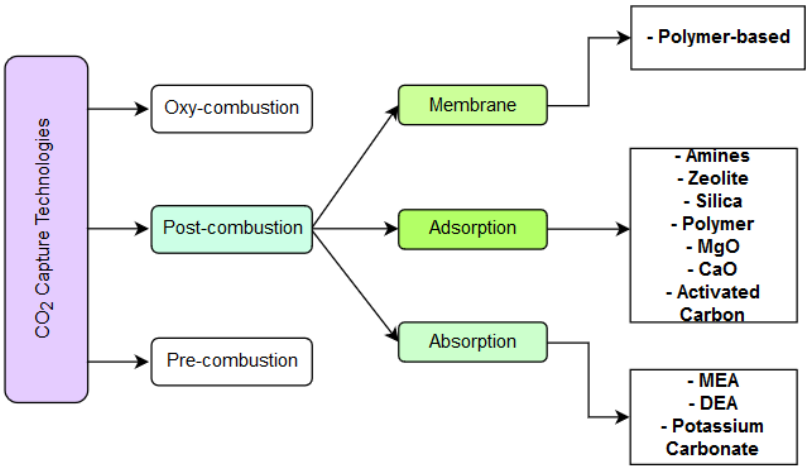

Figure 7. Summary of Post-Combustion CO_2 Capture Technologies.

Post-combustion capture processes can be more easily integrated into existing infrastructure without substantial changes to the basic combustion technology. They are more flexible than pre-combustion capture methods since power plant operations are not contingent on post-combustion capture functionality. Thus, post-combustion capture processes are the leading candidate for CO_2 capture in gas-fired power plants (Herzog, Meldon et al. 2009). However, this introduces the significant challenge of separating CO_2 from the large amount of diluent from combustion in air. Therefore, research efforts focus on advanced membrane systems for membrane separation, solid sorbents for adsorption, and solvents for absorption of dilute CO_2 from air (NETL 2021).

2.1. Membrane Separation

Membrane-based post-combustion capture uses semi-permeable materials that allow for the selective transport and separation of CO_2 from flue gas (NETL 2021). According to Leung et al., the essential part of this process is a composite polymer membrane (Leung, Caramanna et al. 2014). Audus (Audus 2000) and Gielen (Gielen 2003)

developed a highly efficient membrane that achieved 82 % to 88 % CO_2 separation efficiency, and both organic and inorganic materials have been tested by Jingyu et al. (Xu, Jia et al. 2019) and Roussanaly et al. (Roussanaly, Anantharaman et al. 2018) for CO_2 capture.

Advantages of membrane separation include low capital and operating costs (Ji and Zhao 2016). The membrane requires little material to coat and does not need additional facilities such as large pretreatment vessels and solvent storage. The primary maintenance cost for a membrane separation unit is membrane replacement. Another advantage is its simplicity and reliability because the membrane does not show fast decay in performance; it can be running unattended for lengthy periods. It also has no saturation and does not require frequent shutdown and start-up because the gas does not stay and react with the membrane.

However, Brunetti et al. noted that the performance of a membrane system is strongly affected by the flue gas conditions with typically low feed CO_2 concentrations and pressures (Leung, Caramanna et al. 2014). Other obstacles of membrane separation include low permeability and selectivity, poor stability, aging, swelling and sensitivity to the content of impurities and water (Yousef Alqaheem 2017, Jiayou Xu 2019).

2.2. Absorption

The most common post-combustion capture process involves contacting the CO_2-rich flue gas with a reactive solvent cycling between absorption and stripping columns. The CO_2-lean solvent removes CO_2 from the flue gas in the absorber, forming a CO_2-rich

solvent. The CO_2-rich solvent cycles to a stripping column, where CO_2 is desorbed and collected, forming a CO_2-lean solvent that cycles back to the absorber(NRC 2021).

The leading post-combustion CO_2 capture technology uses aqueous monoethanolamine (MEA) mixtures (Herzog, Meldon et al. 2009). Diethanolamine (DEA), methyldiethanolamine (MDEA), and potassium carbonate (K_2CO_3) are also used in post-combustion CO_2 capture technology (Leung, Caramanna et al. 2014). Among the various aqueous alkanolamines, MEA has a low cost, high absorption capacity, and low regeneration heat requirement. However, according to Xue et al., because of the high heat of reaction (~85 kJ/mol CO_2) for CO_2 and MEA, there is a high reaction energy requirement. Other disadvantages being reported include degradation of amines with temperature and time, corrosion, amine losses by evaporation, toxicity of solvents used in absorption processes (Bo Zhao 2011, Budzianowski 2016).

Although structural modifications to the sorbents in MEA-based CO_2 capture processes have decreased cost, modified amines do not meet the environmental and health/safety goals necessary for implementing green-chemistry reagents. Therefore, DEA can be considered for low-pressure operations where the heat of reaction is lower when it reacts with CO_2 (~70 kJ/mol CO_2). Because DEA is much less reactive to sulfur components and its products are much less corrosive, it is a better alternative for CO_2 capture. However, DEA exhibits slow capture kinetics (Xue, Yu et al. 2017).

2.3. Adsorption

In the post-combustion adsorption method, CO_2 molecules are selectively separated from a gas mixture either by forming a chemical bond with the sorbent (i.e.,

chemisorption favored at high temperatures) or by adhering to the adsorbent matrix surface by weak intermolecular forces (i.e., *physisorption favored at lower temperatures*) (Ünveren, Monkul et al. 2017). The sorbent is regenerated by altering its temperature or pressure to shift the CO_2 adsorption equilibrium (called temperature and pressure swing adsorption, respectively).

Alkali metal carbonates like potassium carbonate (K_2CO_3) and sodium carbonate (Na_2CO_3) have been recognized as potential sorbents for CO_2 capture because of their high CO_2 capture capacity and low costs (Yang, Luo et al. 2016). While K_2CO_3 absorbs CO_2 at a relatively slow rate, the reaction rate can be increased through the use of catalytic promoters, such as DEA, arsenic acid, selenous acid, and tellurous acid. However, K_2CO_3 is not an ideal capture material because it requires high operating temperatures (110-115.6 ^oC) and can cause equipment failure due to corrosion (Mokhatab and Poe 2015). According to Yang et al., the regeneration behaviors of alkali metal carbonates can be altered when they are supported on nano porous structural materials, such as activated carbon, aluminum oxide (Al_2O_3), carbon nanofibers, or when combined with titanium(II) oxide (TiO), ferric oxyhydroxide (FeOOH), or magnesium oxide (MgO) (Yang, Luo et al. 2016). In principle, an ideal sorbent should have a high CO_2 adsorption capacity, high selectivity for CO_2, and should be regenerable without significant cyclic performance loss (Ünveren, Monkul et al. 2017).

Although high levels of CO_2 capture are possible with commercially available chemical solvent-based systems, they have significant solvent regeneration energy requirements,

high capital, and operation costs, and degrade significantly with time. Membranes are also viable option, but they have poor stability and sensitivity to impurities. Solid sorbents are being explored for post-combustion CO_2 capture processes that offer advantages over aqueous processes (e.g., lower heat capacity than water). Additionally, solid sorbents have comparably less environmental and health impacts, have high adsorption capacity, low capital investment, and ease of handling (Ziobrowski and Rotkegel 2022). For this reason, solid sorbents are among the most promising candidates for post-combustion CCS. Several environmentally safe solid sorbents are discussed in more detail in the next section (NETL 2021).

Chapter 3: Direct Air Capture Experiment

Direct air capture of CO_2 (DAC) was briefly introduced in Chapter 1.6. above. Capture costs and energy needs related to the technology type was also discussed, including an overview of future plans for implementation. The goal of this thesis as stated above is to explore other absorption systems like amino acids and amino acid salt solutions. In this study, four different amino acids (L-arginine, L-histidine, L-lysine, and glycine) and amino acid salt (potassium salt of L-arginine, potassium salt of L-histidine, potassium salt of L-lysine, and potassium salt of glycine) solutions are investigated for CO_2 absorption and desorption. Their performance as standalone solutions are discussed in comparison to MEA, then the best amino acid solution is studied with different catalysts (SBA-15, Na-3DG, K-3DG, and Mg-3DG) in order to improve its performance.

3.1. Sorbent selection

When selecting absorbents for CO_2 capture, the CO_2 absorption rate, solubility, uptake, stability, environmental safety, and price are all very important factors to consider. The chemistry of absorption is largely controlled by the equilibrium constants of the reactions taking place. Higher equilibrium constants will result in higher heat of absorption, while low equilibrium constant will result in an insignificant amount of CO_2 absorption.

The following absorbents were selected to be studied in comparison to MEA; L-arginine, L-histidine, L-lysine, glycine, and the potassium salt of each of the amino

acids. The structure of each sorbent is shown in Figure 8 below.

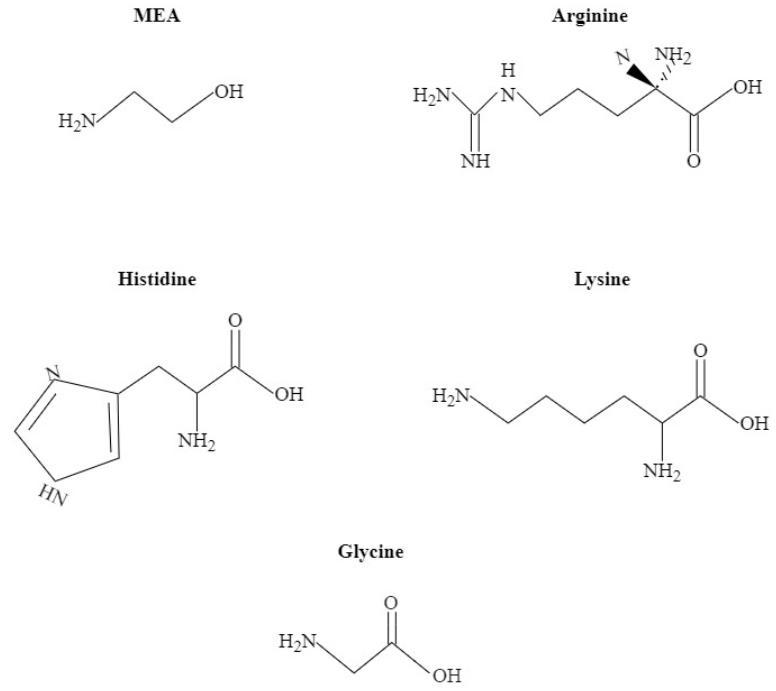

Figure 8. Sorbent Structures.

MEA

MEA is traditional sorbent for CO_2 capture. The technology has been well established over the years. MEA gained its popularity because of its high absorption capacity and fast rate of reaction, but it is corrosive and requires high energy for regeneration. The reaction between CO_2 and an amine solution like MEA is complex, and three reactions in particular are considered (Roongrat Sakwattanapong 2009):

Carbamate formation: $CO_2 + 2RR^INH \leftrightarrow RR^INH_2^+ + RR^INCOO^-$ (1)

Bicarbonate formation: $CO_2 + RR^INH + H_2O \leftrightarrow RR^INH_2^+ + HCO_3^-$ (2)

Carbamate reversion: $CO_2 + RR^INCOO^- + 2H_2O \leftrightarrow RR^INH_2^+ + 2HCO_3^-$ (3)

where *R* represents *-C2H4OH, R′* represents *-H* and *-C2H4OH* for primary and

secondary amines, respectively (Roongrat Sakwattanapong 2009). Different types of amines vary substantially in how they react with CO_2, with respect to both mechanism and kinetics. Tertiary amines (NR_3) differ from primary (RNH_2) and secondary amines (R_2NH), and sterically hindered amines differ from non-sterically hindered amines (Hook 1997, Silva and Falck 2005). MEA is a primary amine.

A number of alkanolamine based sorbents are being studied, including secondary, amines, tertiary amines, and amine blends. However, alkanolamine are inherently problematic due to their volatility, degradation in oxygen rich environments, and formation of toxic degradation products. They are also harmful to human health and easily escape from the solution. Sorbents with more favorable characteristics than MEA are being studied with a goal to find a suitable replacement.

Amino Acids and Amino Acid Salts

Amino acids have the same amine functionality as alkanolamine, as seen in Figure 8 above (Jacco van Holst 2006). Compared to MEA based sorbents, amino acids and amino acid salts are characterized by low vapor pressures and higher stability towards oxidative degradation (P. S. Kumar 2003). They are also environmentally friendly as amino acids are found in nature. During CO_2 absorption in an amino acid salt solution, precipitation could occur, but the precipitation of reaction products means that their concentration in the liquid phase is decreased. This increases the CO_2 absorption by the solvent (Feron 2004).

In order to discuss the possibility of implementing amino acid and amino acid salt

solutions into the process of CO_2 capture, their chemical nature must be discussed and understood. As shown in Figure 8, amino acids have both amine and carboxylic acid functional groups. In biochemistry, amino acid most often refers to α-amino acids with the general structure shown in Figure 9. In α–amino acids, the amine and the carboxylic acid groups are both attached to the α-carbon. The chemical variety of the α-amino acids comes from the difference in the side chain R, which is an organic substituent also attached to the α-carbon (Bruce Alberts 2002).

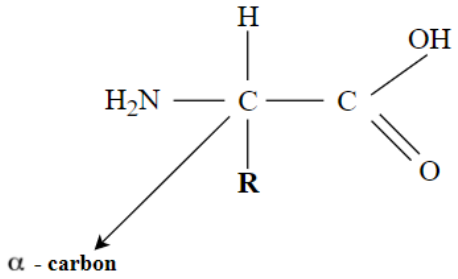

Figure 9. General Structure of α-Amino Acid.

All the standard amino acid except glycine have an asymmetric α-carbon and can thus exist in two stereoisomer forms called L and D enantiomers, but only L-enantiomers are found in proteins (Christopher K. Mathews 1999). One way to group the standard amino acids is according to whether the side chain is basic, acidic, uncharged polar or non-polar. The side chains of Arginine, Histidine, and Lysine are basic, while Glycine is non-polar (Bruce Alberts 2002). Amino acids in water form a zwitterion, as indicated in equation (4). Based on the reaction mechanism of the CO_2 and amino acids, the base form is the active form. Therefore, amino acids need to be deprotonated to react with CO_2 at neutral pH. Some of the bases considered to neutralize amino acids are MEA, KOH, and NaOH. The deprotonation step is necessary in order to make the amine group

reactive toward CO_2 (Hamborg, Niederer et al. 2007, Ciftja 2013, Guo, Thee et al. 2013, Bian, Shen et al. 2016).

$$HO_2CRNH_3^+ \leftrightarrow {}^-OOCRNH_3^+ \leftrightarrow 2H^+ + {}^-OOCRNH_2 \quad (4)$$

Due to the similar functional group between amino acids and alkanolamines, the reaction mechanism of the amino acids can be considered as those of alkanolamines (Sang Sefidi and Luis 2019). Two mechanisms have been proposed to demonstrate the reaction kinetics of CO_2 with the amine group: the zwitterion mechanism and the termolecular mechanism. The reactions of the zwitterion mechanisms are shown in reactions 5-7, and the termolecular reaction of amino acids with CO_2 is described in reaction 8 (Sang Sefidi and Luis 2019). The zwitterion mechanism considers the formation of a zwitterion, and this is followed by the removal of a proton by a base. However, in the termolecular mechanism, an amine reacts simultaneously with one molecule of CO_2 and one molecule of a base (Sang Sefidi and Luis 2019). There are several studies on the kinetic reaction of amino acids, which show that the zwitterion mechanism explains better the kinetic reaction of amino acids. However, the termolecular mechanism better fits the reaction of arginine with CO_2 (Sang Sefidi and Luis 2019).

Zwitterion reaction mechanism:

$$2^-OOCRNH_2 + CO_2 \leftrightarrow {}^-OOCRNHCOO^- + {}^-OOCRNH_3^+ \quad (5)$$

$$^-OOCRNHCOO^- + {}^-OOCRNH_3^+ + H_2O \leftrightarrow + {}^-OOCRNH_3^+ + HCO_3^- + {}^-OOCRNH_2 \quad (6)$$

$$^-OOCRNH_3^+ + HCO_3^- + {}^-OOCRNH_2 \leftrightarrow 2^-OOCRNH_3^+ + CO_3^{2-} \quad (7)$$

Termolecular reaction mechanism:

$$CO_2 + {}^{-}OOCRNH_2 \ldots . B \leftrightarrow {}^{-}OOCRNHCOO^{-} \ldots BH^{+} \quad (8)$$

Amino acids themselves have a slow reaction rate and low CO_2 loading in neutral pH. However, when they are neutralized with a base, their performance enhances significantly. Among the known counterions, KOH shows a higher activity and solubility limit than NaOH and LiOH (Sang Sefidi and Luis 2019), so it is used in this research to produce the amino acid salt.

3.2. Catalysts

Graphene with a surface microporous structure, is one of the most important engineering materials with a variety of applications. It is generally synthesized with valuable hydrocarbons as carbon sources (Sun and Hu 2021). Producing versatile graphene materials directly from CO_2 is exciting and innovative. Additionally, it is important to produce 3D-structured graphene materials, which can avoid the restacking of the graphene sheets and thus keep the graphene properties for practical applications (Sun and Hu 2021). The surface-microporous structure has advantages in the mass diffusion process and exposure of absorption sites for CO_2, achieving high absorption capacity. According to Sun et el., a proven practice is the CO_2 adsorption property of the surface microporous 3D graphene produced via the reaction between Na and CO_2 at 500−700 °C. The large surface area (700−900 m^2 g^{-1}) and the surface microporous structure allow efficient mass diffusion and provide abundant adsorption sites. As a

result, a maximum adsorption capacity of 2.28 mmol g^{-1} was achieved at 298 K and 1 bar (Sun and Hu 2021). The adsorption capacity was increased further to 3.13 mmol g^{-1} after the optimal 3D graphene material was activated by KOH which could introduce more oxygen functional groups (Sun and Hu 2021).

SBA-15 is a mesoporous silica sieve with a microporous surface just like 3D-graphenes (3DG). It has been chosen to be studied because of its mesostructured surface. SBA-15 has surface area of typically 400-900 $m^2 \cdot g^{-1}$, high thermal and mechanical stability, inert, and not harmful to the environment (Quach Nguyen Khanh Nguyen 2020). This makes SBA-15 a well-suited material for various applications like a catalyst in CO_2 capture. According to Nguyen et al., it can be used in environmental treatment for adsorption and separation, and as a support material for catalysts. It can also be used as a template for the production of ordered mesoporous carbon (Quach Nguyen Khanh Nguyen 2020). SBA-15 and 3DG have similar properties and advantages for CO_2 capture, so they are being directly compared to one another in this research to determine how their utilization in addition to amino acids affects CO_2 capture capacity.

Chapter 4: Materials and methods

4.1. Solution and Catalyst Preparation

The absorbents used in the experiment as previously mentioned includes the solutions of; MEA, L-arginine, L-histidine, L-lysine, glycine, and the potassium salts of L-arginine, L-histidine, L-Lysine, and glycine. The catalysts are; SBA-15, Na-3DG, K-3DG, and Mg-3DG. Other equipment and materials are discussed in the next section.

MEA reagent purchased from ACROS Organics was used. The crystalline powders of l-arginine, l-histidine, l-lysine, glycine were used as precursors for the amino acid absorbents, and potassium hydroxide flakes used in addition to the amino acids as precursors for the amino acid salt absorbents. The detailed method of preparation of the sorbent solution is discussed next.

MEA

10 mmol MEA was used as the concentration of the sorbent during the experiment. It was prepared by weighing out 0.6108 g of the MEA reagent, then mixed with 40 ml deionized (DI) water and poured into the reaction tube.

Amino Acids

10 mmol amino acids (of l-arginine, 99.89 % l-histidine, 95 % l-lysine, and 99 % l-glycine) were used for each of the sorbent solutions during this stage of the experiment. For each separate solution, 1.742 g of l-arginine, 1.552 g of l-histidine, 1.7284 g of l-lysine, 0.7583 g of glycine, was mixed with 40 ml DI water to create 10 mmol l-arginine, 10 mmol l-histidine, 10 mmol l-lysine, and 10 mmol glycine respectively.

Amino Acid Salts

10 mmol potassium salt (of l-arginine, 99.89 % l-histidine, 95 % l-lysine, and 99 % l-glycine) was used for each of the sorbent solutions during this stage of the experiment. For each separate solution, the same amount of amino acids mentioned above was used, in addition to 0.6234 g of potassium hydroxide (KOH).

To prepare each solution, 0.6234 g KOH was dissolved in 10 ml DI water, it was then mixed in each case with 1.742 g of l-arginine, 1.552 g of l-histidine, 1.7284 g of l-lysine, 0.7583 g of glycine, which was already dissolved in 30 ml DI water to create 10 mmol l-arginine salt, 10 mmol l-histidine salt, 10 mmol l-lysine salt, and 10 mmol glycine salt respectively.

Catalysts

The 3DG catalysts were prepared in the lab, while the SBA-15 catalyst was purchased from a commercial supplier Sigma-Aldrich. 99 % SBA-15 with trace metal basis was prepared by the hydrothermal method. 3DG catalysts were prepared through the reaction of CO_2 gas with alkali metals; Na, K, and Mg. 50 mmol Na, K or Mg, metal was briefly loaded into a ceramic tube batch reactor and CO_2 was introduced into the reactor with the initial pressure of 50 psi at room temperature. Followed by the reactor being heated to 600 ℃ for 24 h, respectively, which are denoted as Na-3DG, K-3DG, Mg-3DG. The obtained graphene was separated from solid products by HCl treatment (36.5 wt. %), deionized water washing (>10 times) and centrifugation. The samples as obtained were dried overnight at 80 ℃. 3DG with different diameters, shape and surface-microporous were obtained by changing the type of metal raw material used.

4.2. Equipment Configuration

A figure of the experiment setup is shown below. The following ProSpec specialty gases from Praxair were used for every experimental run: 100 % nitrogen (N_2), N_2 with 404 ppm CO_2 , and a mixture of 10 % CO_2 and 90 % N_2. A red-y smart series mass flow controller (MFC) is used to control the flow rate of the inlet gases into the solution and/or gas analyzer. The CAI ZPA gas analyzer is used to measure the concentration of CO_2 in the gas stream, and it is connected to a Monarch DataLogger that records and stores the data for further analysis. One of the channels in the gas analyzer measures CO_2 concentration in ppm (maximum. 1000ppm), and the other channel measures CO_2 concentration in vol% (maximum 50 vol%). The thermocouple shown in Figure 10 below is also connected to the DataLogger to record the temperature data. The cold-water bath is controlled by a Thermo Neslab Digital Plus RTE-17 chiller. It is a refrigerated bath circulator that runs through the condenser, keeping it at 5 °C throughout the experiment.

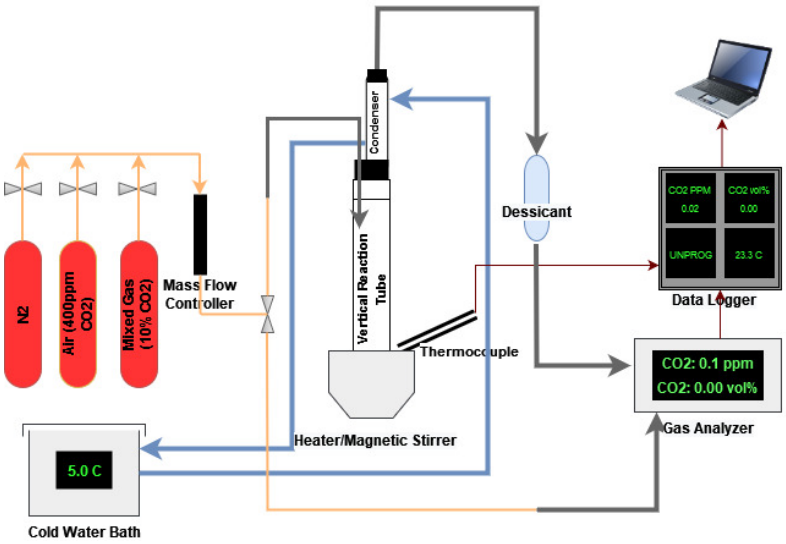

Figure 10. Experiment Setup.

4.3. Air capture process

Absorption

The first stage of the experiment involves CO_2 absorption for 6 hours at room temperature (20-25 ºC), and 1 atm. The gas tanks all have their regulators set to 100 psi. To start the experiment, the chiller is turned on to start cooling the cold-water bath, the computer is also booted on to start the get red-y software that controls the red-y MFC and set to a flowrate of 500 ml/min for the entire duration of the experiment. After this, the N_2 valve is opened completely to purge the flow lines directly connected to the gas analyzer. Once the reading on the gas analyzer is stable (~2 minutes) it is zeroed to establish a reading of 0 ppm (channel 1) and 0 vol% (channel 2) CO_2. The N_2 valve is then closed and the valve controlling the opening of the N_2 with 404 ppm CO_2 tank is opened completely. The gas also flows directly to the gas analyzer at this stage, to establish a reading of 404 ppm CO_2 in channel 1, the reading for channel 2 is not calibrated at this time because the data is not used. After calibrating channel 1 on the gas analyzer, the lines are purged again with N_2 gas to get the reading back to 0 ppm. After the calibration of the gas analyzer and DataLogger, the absorption solution is prepared.

In other to prepare the solution, a specified amount of absorbent is measured, the measurements and preparation were discussed Chapter 4.1. above. For example, a solution of 10 mmol l-lysine requires 1.7284 g l-lysine, mixed with 40 ml DI water. A solution of 10 mmol l-lysine salt requires 1.7284 g l-lysine and 0.6234 g KOH, mixed with 40 ml DI water. When a catalyst is required, that is also weighed out and added to

the reaction tube before the solution. After measuring and preparing the solution, it is poured into the vertical reaction tube which is then sealed with a rubber stopper. The stopper has holes drilled into it to allow for a condenser and a small tube for inlet gas flow. Once the reaction column is properly connected and sealed, the solution is purged with N_2 gas also at 500 ml/min, until the gas analyzer reads ~0 ppm, and after this the experiment is ready to begin.

During absorption, N_2 gas with 404 ppm CO_2 flows through the MFC at 500 ml/min and into the vertical reaction tube containing 40 ml solution where the CO_2 is absorbed. It then flows through the condenser, and through a small desiccant tube before reaching the gas analyzer where the unabsorbed CO_2 concentration in the effluent gas is measured for a total experiment time of 6 hours. When the experiment ends, the valve for N_2 gas with 404 ppm CO_2 is closed completely, and the MFC is set to 0 ml/min. The data is downloaded from the DataLogger, and exported into excel for calculations and graphs, then the desorption stage is ready to be started.

Desorption

The second stage of the experiment involves CO_2 desorption for 1 hour at (70 ^oC) and 1 atm. The gas tanks all have their regulators set to 100 psi.

After absorption is completed and the data has been exported, the desorption step is ready to be started. First the desiccant is replaced if the first one is completely spent. Then the vertical reaction tube is placed in a small water bath in the heater, to bring the temperature up to 70 ^oC. After this, the thermocouple is placed into the water bath to monitor the temperature throughout the experiment, and the magnetic stirrer is set to

400 rpm.

The gas analyzer and DataLogger have to be calibrated again during desorption. N_2 valve is opened completely to purge the flow lines directly connected to the gas analyzer of CO_2. Once the reading on the gas analyzer is stable (~2 minutes) it is zeroed to establish a reading of 0 ppm (channel 1) and 0 vol% (channel 2) CO_2. The N_2 valve is then closed and the valve controlling the opening of the 10 % CO_2 tank is opened completely. The gas also flows directly to the gas analyzer to establish a reading of 10 vol% CO_2 in channel 2, the reading for channel 1 is not calibrated because the data is not used. After calibrating channel 2 on the gas analyzer, the lines are purged again with N_2 gas to get the reading back to 0 vol%.

After the calibration of the gas analyzer and DataLogger, the experiment is started. N_2 is set to flow through the solution at 500 ml/min for 1 hour. During this time the solution is heated to 70 ^oC by the heater, and CO_2 is desorbed and measured in the effluent gas by the gas analyzer. When the experiment ends, the valve is closed completely, and the MFC is set to 0 ml/min. The data is downloaded from the DataLogger and exported into excel for calculations and graphs.

4.4. Catalyst characterization

3D-Graphenes (3DG)

The catalyst preparation methods have been discussed above. The 3DG catalyst samples were characterized by X-ray diffractometer (XRD, SHIMADZU XDS-6100), equipped with Cu Kα (λ=1.5406 Å) radiations. The specific surface area (SSA) was

measured by using a Micromeritics ASAP 2020 surface area measurement analyzer, which measured N_2 adsorption and desorption isotherms at a liquid-nitrogen temperature (77 K). Before N_2 adsorption and desorption measurements, the sample was degassed at 250 ℃. The morphology and elemental distribution were studied by field emission scanning electron microscope (FESEM) and energy-dispersive X-ray spectrometry (EDS) with a ZEISS SUPRA 55VP scanning electron microscope (SEM), equipped with BRUKER X Flash Detector 5010. The high-resolution transmission electron microscopy (HRTEM) and selected-area electron diffraction (SAED) were obtained by using an FEI Tecnai G2 F20 transmission electron microscope (TEM), equipped with a field emission gun and operated at 200 kV. Raman analysis was performed by using a LabRAM HR Evolution Raman microscope with a 532 nm laser. X-ray photoelectron spectroscopy (XPS) was carried out on a Thermo K-Alpha.

XRD measurements of products from Na, K, Mg and CO_2 reaction are shown in Figure 11Figure 11 a-c, and the by-products were Na_2CO_3, K_2CO_3, MgO. Additionally, the production of carbon nano walls from the reaction was confirmed as follows: black solid powder was obtained by removing by-products using hydrochloric acid and DI water. As shown in Figure 11 d, all three samples exhibit a relatively strong diffraction peak at 2θ = 24-25.1° and 43.4-45°, which is associated with the (002) diffraction line from hexagonal graphite (JCPDF No: #65-6212). The corresponding d-spacings measured for Na-3DG, K-3DG and Mg-3DG are 3.723, 3.419, and 3.359A˚, respectively. This indicates that the carbon material possesses a layer structure. Also, the average interlayer space of the material is 3.56 Å, which is larger than the interlayer

space of graphite.

Therefore, it can be concluded that the reaction between Na K, Mg and CO_2 gas produced 3D carbon nanoballs at 600 °C as follows:

$$4Na+3CO_2 \rightarrow 2Na_2CO_3 + C \quad (9)$$

$$4K+3CO_2 \rightarrow 2K_2CO_3 + C \quad (10)$$

$$2Mg+CO_2 \rightarrow 2MgO+C \quad (11)$$

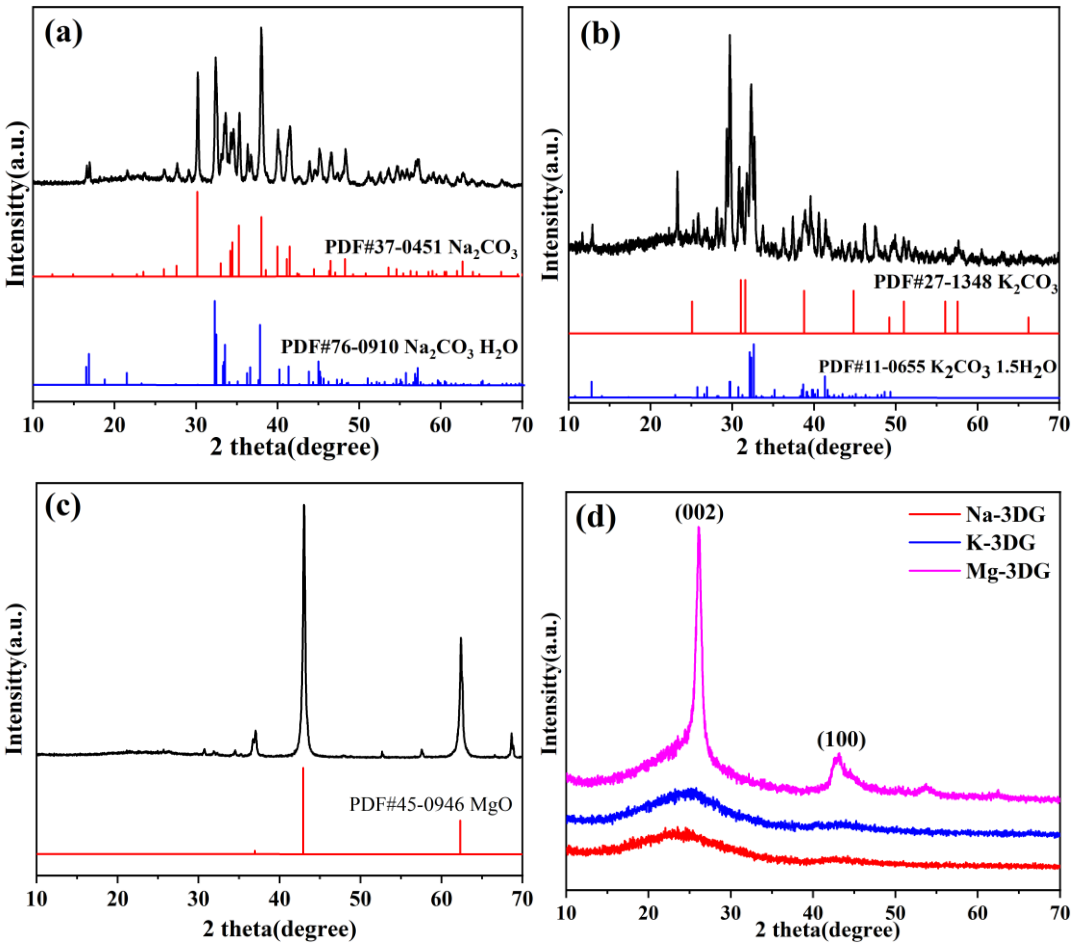

Figure 11. XRD Patterns of Solid Products Before HCl Treatment From the Reaction Between (a) Na and CO_2; (b) K and CO_2; (c) Mg and CO_2; (d) Solid Products After HCl Treatment.

The scheme for synthesis of 3DGs is illustrated in Figure 12. The structure of carbon nanomaterials obtained from the CO_2 reaction is heavily dependent on the reactive

metal, which can be explained as follows: For Na and K, the stacking rate of graphene sheets to graphite is faster than the generation of by-product particles (Na_2CO_3/K_2CO_3), leading to the formation of large flakes. In contrast, using Mg as the raw material, the generation of MgO particles is fast enough to separate graphene sheets and thus inhibits their stacking. Consequently, 3D flower-structured graphene could be obtained using Na and K. So, we can conclude that the structure of carbon nanomaterials can be tuned by changing the reactive metal for the synthesis reaction.

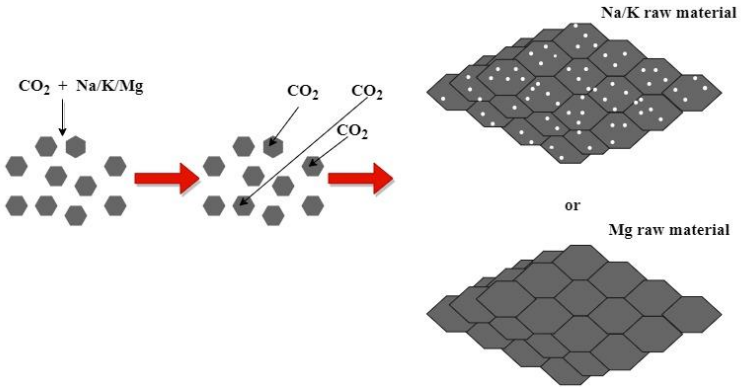

Figure 12. Schematic Illustration of the Preparation of 3DGs.

The morphology of the carbon material was evaluated by FESEM, shown in Figure 13 a. When Na was employed, the synthesized graphene sheets possessed a 3D honeycomb shape (with cell size in the range of 50–100 nm). Though, when the K was used, the shape of the synthesized 3D graphene changed. A plate-like structured graphene was obtained from the reaction of CO_2 with K, shown in Figure 13 b. Additionally, when the Mg is used as the raw material, the obtained graphene exhibited a granulated shape Figure 13 c. This indicates that the shape of 3D graphene could be tuned by changing reactive metal.

The EDS results of the powder proved that it was carbon material with some oxygen

functional groups, shown in Table 1. Raman spectras are show in Figure 13 d, the D band at 1355 cm^{-1}, which corresponds to the disordered sp2 carbon generated by linking with sp3 carbon atoms, and a G band at 1575 cm^{-1}, which is associated with the stretching of sp2 carbon pairs. The integrated intensity ratio of the D band to the G band (which can be used as the degree of disorder) of Na-3DG, K-3DG and Mg-3DG is 0.86, 1.14, and 0.73, respectively.

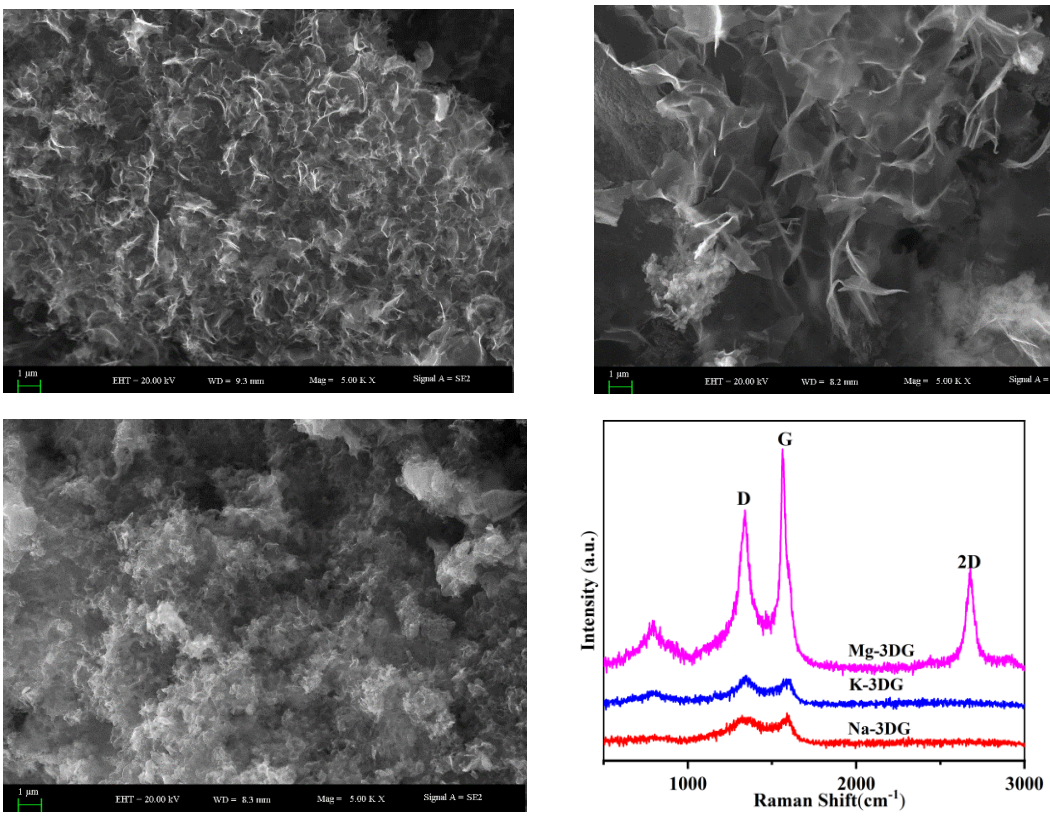

Figure 13. SEM Images of: (a) Na-3DG, (b) K-3DG and (c) Mg-3DG Samples; (d) Raman spectra of as-synthesized 3DGs.

Table 1. Composition of as-synthesized 3DGs.

	Raman	EDS	
Sample name	I_D/I_G	C (mol %)	O (mol %)
Na-3DG	0.86	95.08	4.92
K-3DG	1.14	95.06	4.94
Mg-3DG	0.73	92.08	7.92

The specific surface area and porous structure of 3DGs were determined by N_2 adsorption/desorption isotherms at 77 K. The adsorption/desorption curves can be fitted with a type-II and type-IV isotherm as seen in Figure 14 a-c, which indicates the microporous structure of as-synthesized 3DGs. The specific surface area of 765.5, 391.2 and 643.4 $m^2 \cdot g^{-1}$ has been rendered by Na-3DG, K-3DG and Mg-3DG samples, respectively. The pore size distribution was obtained from the t-plot method and summarized in Table 2. The micropore area of 650.2, 209.5 and 0 $m^2 \cdot g^{-1}$ has been measured for Na-3DG, K-3DG and Mg-3DG samples, respectively. The calculated average micropore size was 6.9-8.0 Å, which was obtained from Horvath–Kawazoe pore size analysis. The Na-3DG and K-3DG exhibited an abundant number of surface micropores. Furthermore, the surface micropores may be originated from *in-situ* oxidization of graphene walls due to CO_2 .

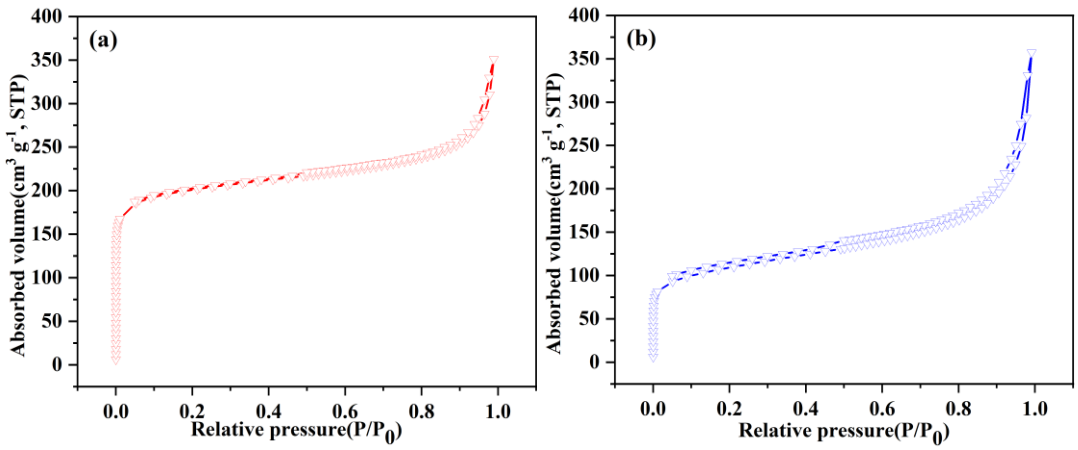

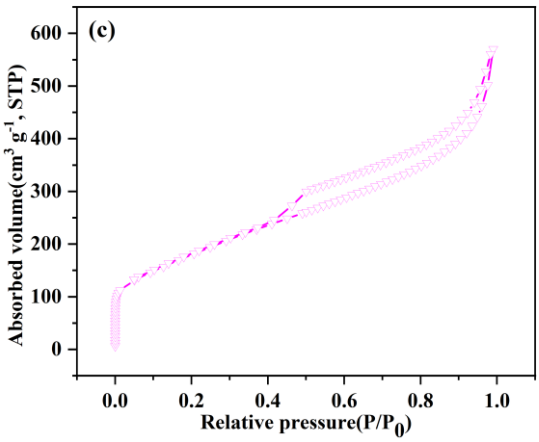

Figure 14. N_2 Adsorption/Desorption Curves at 77 K of (a) Na-3DG, (b) K-3DG and (c) Mg-3DG Samples.

Table 2. Specific Surface Area, Pore Size Distribution and Porous Structure Characterization Results of as-synthesized 3DGs.

Sample name	Specific surface area (m^2 g^{-1})	Micropore area (m^2 g^{-1})	External surface area (m^2 g^{-1})	$S_{micropores}/S_{total}$	Average diameter of micropores (Å)
Na-3DG	765.5	650.2	115.3	84.9%	6.9
K-3DG	391.2	209.5	181.7	53.6%	8.0
Mg-3DG	643.4	0	643.4	0%	-

SBA-15

The characterization for the SBA-15 catalyst was provided by a chemical supplier ACS Material. The widely available technical data sheet contains all the information listed below. The characterization of SBA-15 is shown in Table 3. The appearance of the catalyst is described as a white powder, a range of values are also given for the typical particle size and pore diameter of SBA-15.

Table 3. The Characterization Results of SBA-15.

Property	Value
Appearance	White Powder
Particle Size (μm)	1-4
Pore Diameter (nm)	6-11

Pore Volume ($cm^3\ g^{-1}$)	1.46
BET Surface Area ($m^2\ g^{-1}$)	≥ 550
Na_2O (%)	≤ 0.1
Comparative Crystallinity (%)	≥ 90
Bulk Density ($g\ cm^{-3}$)	0.067
Tap Density ($g\ cm^{-3}$)	0.145

The typical SEM, TEM, XRD analysis, and BET analysis of ACS Material SBA-15 is shown in Figure 15 a-b, Figure 16 a-b, Figure 17, and Figure 18 respectively.

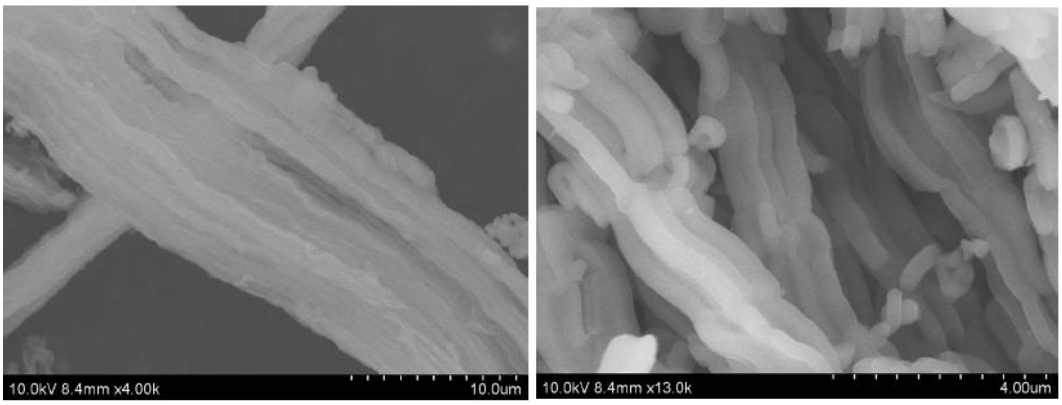

Figure 15. (a)-(b) Typical SEM Images of ACS Material Mesoporous Silica Molecular Sieve SBA-15.

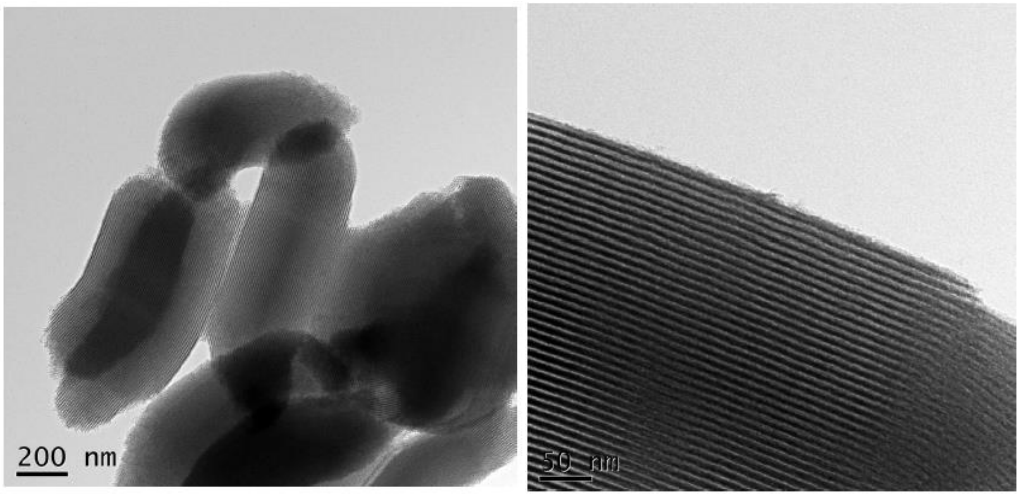

Figure 16. (a)-(b) Typical TEM Images of ACS Material Mesoporous Silica Molecular Sieve SBA-15.

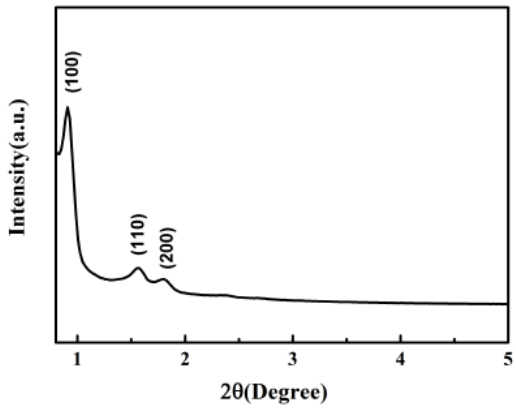

Figure 17.Typical XRD Analysis of ACS Material Mesoporous Silica Molecular Sieve SBA-15.

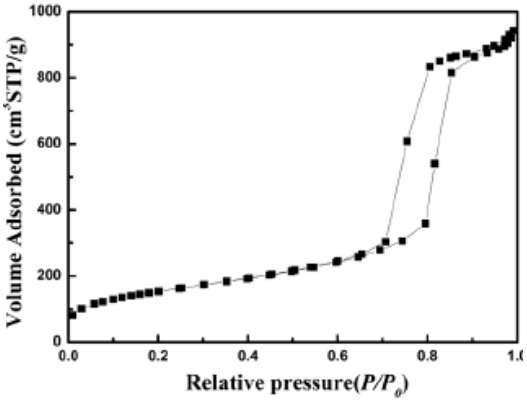

Figure 18.Typical BET Analysis of ACS Material Mesoporous Silica Molecular Sieve SBA-15.

Chapter 5: Results

The results from all the experiments is shown in the subsections below. To start, the cumulative absorption, cumulative desorption, absorption concentration, and desorption concentration of MEA is compared to that of the amino acids (l-arginine, l-histidine, l-lysine, and glycine). Then the same results stated previously are also analyzed for MEA, in comparison to the amino acid salt (l-arginine salt, l-histidine salt, l-lysine salt, and glycine salt). From those results, the best absorbent is chosen with respect to cumulative absorption, cumulative desorption, and breakthrough time, and used for DAC with four different catalysts (SBA-15, Na-3DG, K-3DG, and Mg-3DG). After conducting those experiments, the catalyst with the best absorption, desorption, and breakthrough time is studied further at different ratios with the absorbent.

The cumulative absorption/desorption is the amount of CO_2 absorbed by- or desorbed from the solution over time. The absorption concentration is the amount of CO_2 in the effluent gas, detected by the gas analyzer. This is the measure of CO_2 not absorbed by the solution. The desorption concentration is the amount of CO_2 in the effluent gas, detected by the gas analyzer during desorption. The breakthrough time is found on the absorption concentration graph, it is used to understand the capacity of the absorbent. Longer breakthrough times indicate higher absorption capacity of the absorbent as will be made evident in the sub-sections below.

The absorption and desorption amounts are calculated as follows:

Absorption

Symbols and notations:

$CO_{2,\,ppm}$; CO_2 concentration in ppm from DataLogger

$CO_{2,\,vol\%}$; CO_2 concentration in vol% from DataLogger

$CO_{2,\,feed}$ (ml/min); CO_2 flowrate

$CO_{2,\,feed}$ (mmol/s); CO_2 flowrate

$N_{2,\,feed}$ (ml/min); N_2 flowrate

$N_{2,\,feed}$ (mmol/s); N_2 flowrate

Feed; 404 ppm CO_2 and N_2 balance

$$CO_{2,vol\%} = \frac{CO_{2,ppm}}{10000}$$

$$O_{2,feed} = 0$$

$$N_{2,feed}\left(\frac{ml}{min}\right) = 499.789\ \frac{ml}{min}$$

$$N_{2,feed}\left(\frac{mmol}{s}\right) = N_{2,feed}\left(\frac{ml}{min}\right) * \frac{1\ (atm)}{R\left(\frac{L\,atm}{K\,mol}\right) * T\ (K) * \frac{1}{60\ s}}$$

$$CO_{2,feed}(\frac{ml}{min}) = 0.202\,\frac{ml}{min}$$

$$CO_{2,feed}\left(\frac{mmol}{s}\right) = CO_{2,feed}\left(\frac{ml}{min}\right) * \frac{1\ (atm)}{R\left(\frac{L\,atm}{K\,mol}\right) * T\ (K) * \frac{1}{60\ s}}$$

$CO_{2\ ,in}$; $amount\ of\ CO_2\ in\ the\ feed\ stream$

$$CO_{2\ ,in} = \frac{CO_{2,feed}\left(\frac{mmol}{s}\right)}{CO_{2,feed}\left(\frac{mmol}{s}\right) + N_{2,feed}\left(\frac{mmol}{s}\right)}$$

$$Total\ flowrate\ \left(\frac{mmol}{s}\right) = \frac{N_{2,feed}\left(\frac{mmol}{s}\right)}{\frac{100 - CO_{2,vol\%}}{100}}$$

$CO_{2,out}$; $amount\ of\ CO_2\ in\ the\ effluent\ gas$

$$CO_{2,out}\left(\frac{mmol}{s}\right) = \frac{CO_{2,vol\%}}{100} * Total\ flowrate\ \left(\frac{mmol}{s}\right)$$

$$CO_{2,absorbed}(mmol) = CO_{2\ ,feed}(mmol) - CO_{2,out}(mmol)$$

Desorption

Symbols and notations:

$CO_{2,\ vol\%}$; CO_2 concentration in vol% from DataLogger

$CO_{2,\ feed}$ (ml/min) or (mmol/s); 0

$O_{2,\ feed}$ (ml/min) or (mmol/s); 0

$N_{2,\ feed}$ (ml/min); 500 ml/min

$N_{2,\ feed}$ (mmol/s); N_2 flowrate

Feed; 500 ml/min N_2

$$N_{2,feed}\left(\frac{ml}{min}\right) = 500\ \frac{ml}{min}$$

$$N_{2,feed}\left(\frac{mmol}{s}\right) = N_{2,feed}\left(\frac{ml}{min}\right) * \frac{1\ (atm)}{R\left(\frac{L\ atm}{K\ mol}\right) * T\ (K) * \frac{1}{60\ s}}$$

$$Total\ flowrate\ \left(\frac{mmol}{s}\right) = \frac{N_{2,feed}\left(\frac{mmol}{s}\right)}{\frac{100 - CO_{2,vol\%}}{100}}$$

$$CO_{2,out}\left(\frac{mmol}{s}\right) = \frac{CO_{2,vol\%}}{100} * Total\ flowrate\ \left(\frac{mmol}{s}\right)$$

$$CO_{2,desorbed}(mmol) = CO_{2\ ,out}(mmol) - CO_{2,feed}(mmol)$$

5.1. MEA, L-Arginine, L-Histidine, L-Lysine, and Glycine

As mentioned in sub-Chapter 4.1. above, 10 mmol MEA was used as the basis for comparison for the experiments. It was initially compared to 10 mmol amino acids; l-arginine, l-histidine, l-lysine, and glycine. The cumulative absorption and absorption concentration results are shown in Figure 19 and Figure 20. From the figures, it can be

observed that MEA has a much higher absorption capacity and much better absorption rate. The cumulative absorption after 6 hours was found to be 2.768 mmol CO_2 , with a breakthrough time of 3.95 hours. It has been established that MEA is a popular sorbent for CO_2 capture because of its high absorption capacity and fast rate of reaction, so these results are expected.

After MEA, l-lysine showed the next best CO_2 absorption capacity and breakthrough time, 2.188 mmol and 0.95 hours. Followed by l-arginine with a cumulative absorption of 2.128 mmol and a breakthrough time of 0 hours. Then glycine with cumulative absorption of 0.011 mmol and a breakthrough time of 0 hours, and l-histidine absorbing 0 mmol CO_2 with a breakthrough time of 0 hours.

L-lysine proved to be the best choice of amino acid when compared to the other, while l-histidine proved to be the worst at absorbing CO_2 at that concentration, making it the least likely choice to pursue for this research.

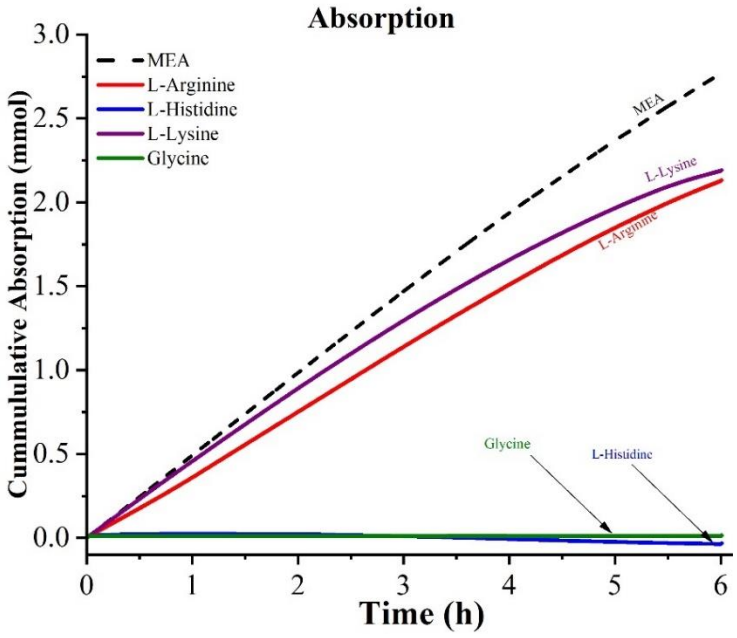

Figure 19. Cumulative Absorption MEA and Amino Acids.

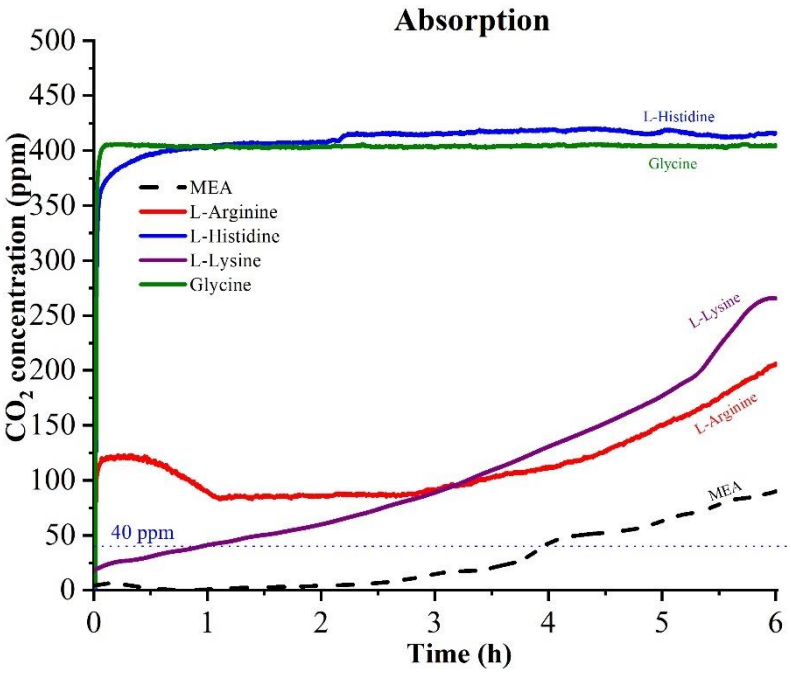

Figure 20. Absorption Concentration MEA and Amino Acids.

The desorption results seemed to be a lot more intriguing than the absorption results. This part of the experiment was operated at 95 ºC. It was observed that l-lysine had the highest cumulative desorption at 2.592 mmol and desorption rate. MEA was a close second with a cumulative desorption of 2.416 mmol, followed by l-arginine at 1.969 mmol. As expected, l-histidine and glycine had the lowest desorption amounts at 0.059 mmol and 0.037 mmol respectively. These results are evident in Figure 21 and Figure 22. Figure 23 provides a summary of the cumulative absorption and desorption in a bar graph.

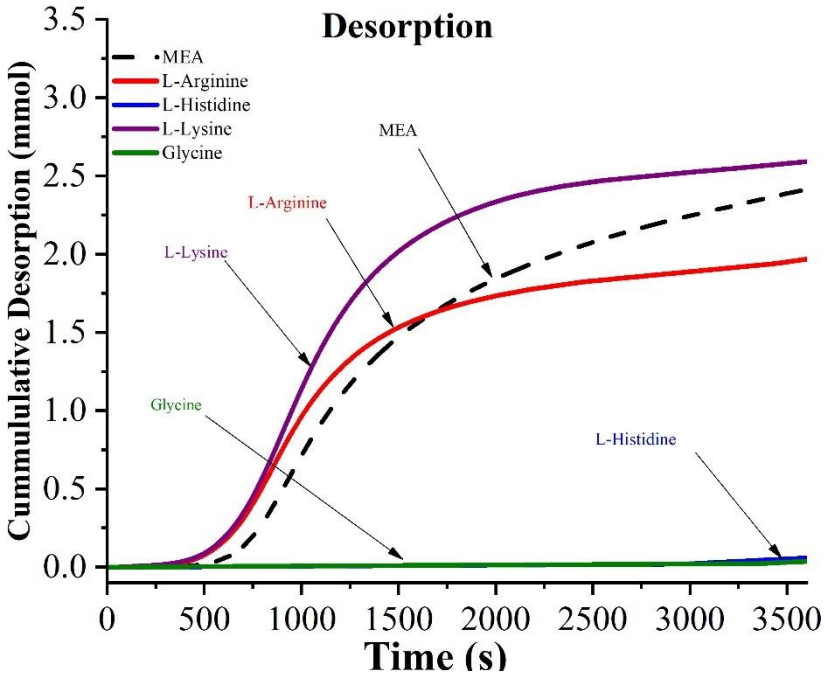

Figure 21. Cumulative Desorption MEA and Amino Acids.

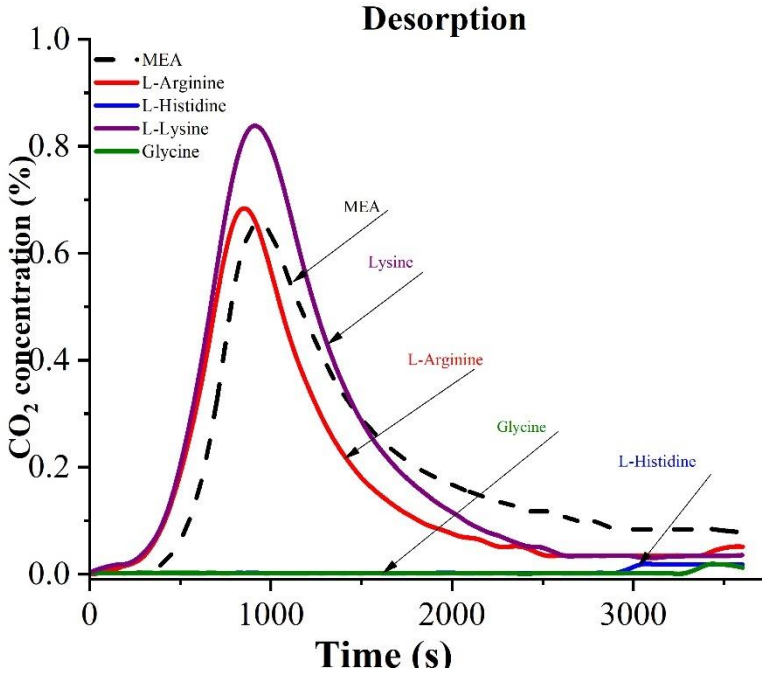

Figure 22. Desorption Concentration MEA and Amino Acids.

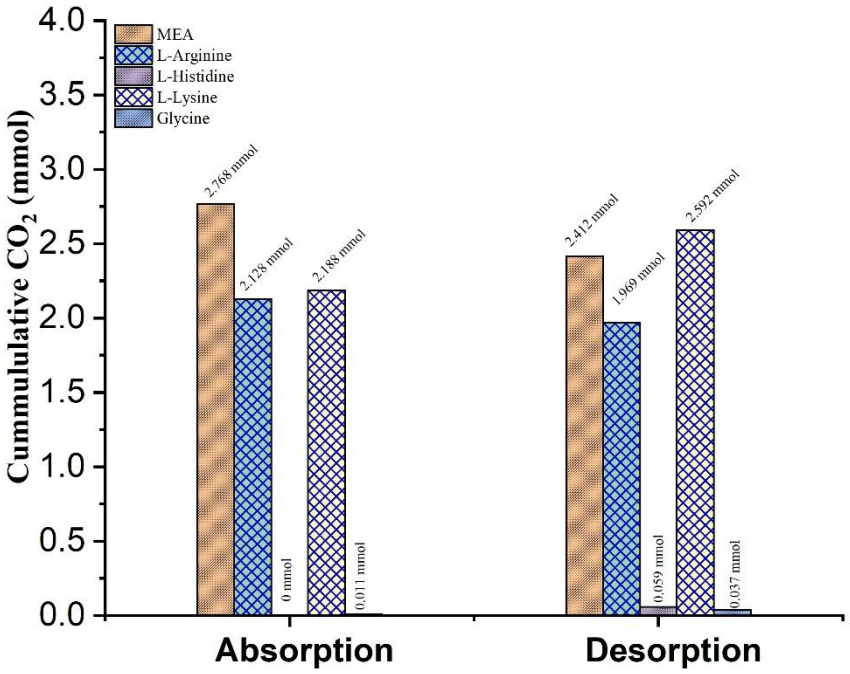

Figure 23. Cumulative Absorption and Desorption Amount MEA and Amino Acids.

During these experiments and all that followed, it was observed that the cumulative amount of CO_2 desorbed is greater than the cumulative amount absorbed for the amino acids. The reason for this phenomenon could be explained by the precision of the channel 2 on the gas analyzer and DataLogger being different from the precision of channel 1, meaning that the data generated would be affected by the precision of the instruments. It could also be explained by the fact that the carboxyl group (COOH) on the amino acids was broken down during the experiment to generate additional CO_2, which is the more likely scenario. This reaction is known as decarboxylation. It is a chemical reaction that removes a carboxyl group and releases CO_2, shown in reaction 16 below.

$$R - COOH \rightarrow R - H + CO_2 \quad (16)$$

5.2. MEA, L-Arginine Salt, L-Histidine Salt, L-Lysine Salt, Glycine Salt

The next set of experiments after comparing MEA with amino acids involved the comparison of MEA with amino acid salts. As discussed briefly in Chapter 3.1., the absorption capacity of amino acids significantly improves when neutralized by a base like KOH. This is evident in the absorption graph shown below (see Figure 24). All the amino acid solutions showed a marked improvement in absorption after the addition of potassium hydroxide (KOH). L-lysine salt showed the highest absorption capacity with a cumulative absorption of 2.909 mmol, although the breakthrough time as seen in Figure 25 was much greater than the 6 hours the experiment ran for. After l-lysine salt, l-arginine salt showed the next best absorption capacity with a cumulative absorption of 2.895 mmol. It also followed the same trend as l-lysine salt, with a breakthrough time also greater than 6 hours. As expected MEA also has a high absorption capacity, right after l-arginine salt. The cumulative absorption was 2.768 mmol, with a breakthrough time of 3.95 hours. After MEA, glycine salt has the next best absorption capacity with a cumulative absorption of 2.715 mmol and a breakthrough time of 3.92 hours. For this set of experiments, l-histidine salt had the lowest absorption capacity and breakthrough time, with a cumulative amount of 2.277 mmol CO_2 and 2.07 hours breakthrough time.

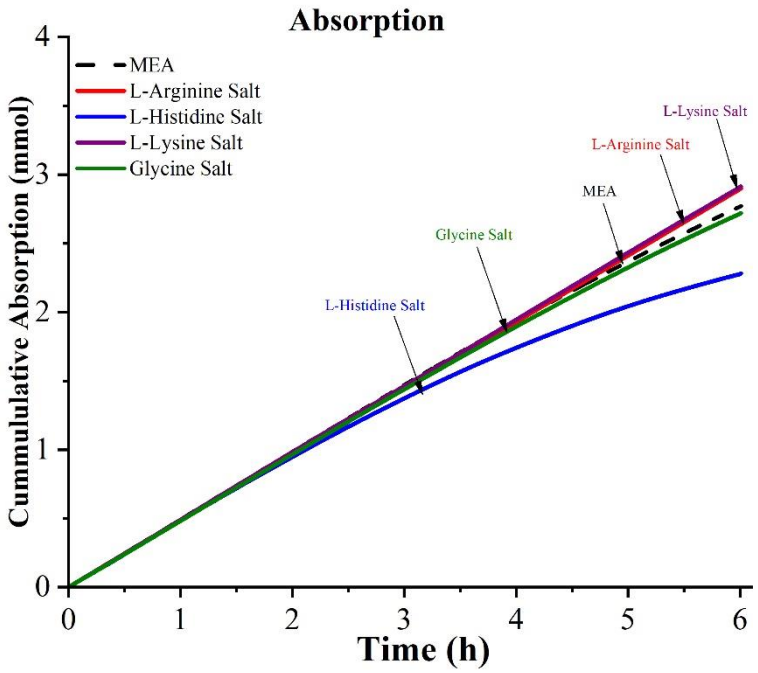

Figure 24. Cumulative Absorption MEA and Amino Acid Salt.

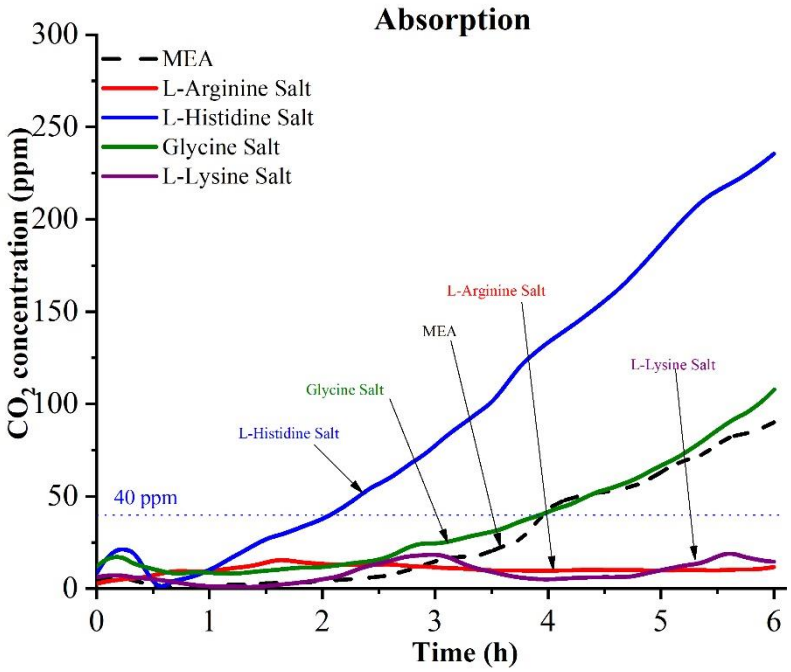

Figure 25. Absorption Concentration MEA and Amino Acid Salt.

This desorption experiment was also operated at 95 °C, and the results were interesting. MEA had the highest desorption amount at 2.416 mmol, followed by glycine salt at 1.974 mmol, then l-histidine salt at 1.944 mmol. L-lysine salt had the second lowest

cumulative desorption amount at 1.283 mmol, followed by l-arginine salt at 0.085 mmol. It was noteworthy to see that the two amino acid salt solutions that absorbed the most CO_2 , desorbed the lowest amount of CO_2. All of this is shown in Figure 26, Figure 27, and Figure 28 below.

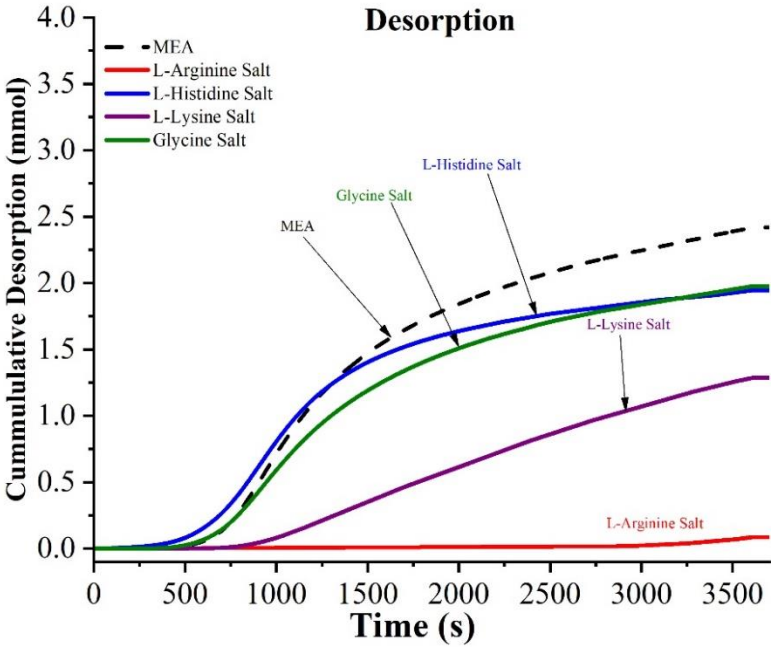

Figure 26. Cumulative Desorption MEA and Amino Acid Salt.

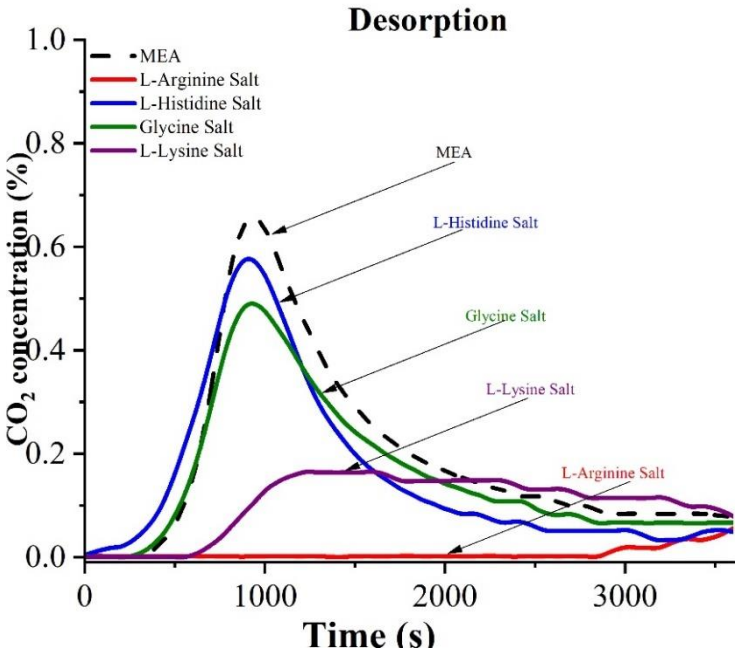

Figure 27. Desorption Concentration MEA and Amino Acid Salt.

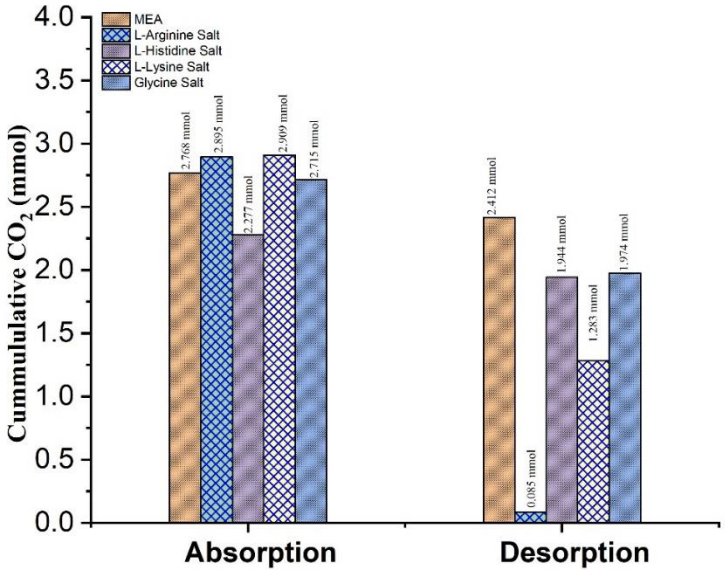

Figure 28. Cumulative Absorption and Desorption Amount MEA and Amino Acid Salt.

After discovering the high absorption and desorption capacity of lysine salt, a longer experiment (about 15 hours) was conducted to find the breakthrough time. The cumulative absorption and desorption was found to be 6.84 mmol and 4.38 mmol respectively, with a breakthrough time of 10.85 hours. All of this is shown in Figure 29, Figure 30, Figure 31, Figure 32 below.

Although l-lysine salt has the highest absorption capacity so far, the breakthrough time is far too long to be feasible for this research. After more testing, the breakthrough time was found to be ~11 hours. The absorption capacity, desorption amount, and breakthrough time for all amino acid and amino acid salt experiments were studied and compared, the conclusion made was to further study l-lysine as the primary absorbent. It has a high absorption capacity, high desorption amount and a breakthrough time that does not hinder implementation. The results of the next stage of experiments are

discussed next.

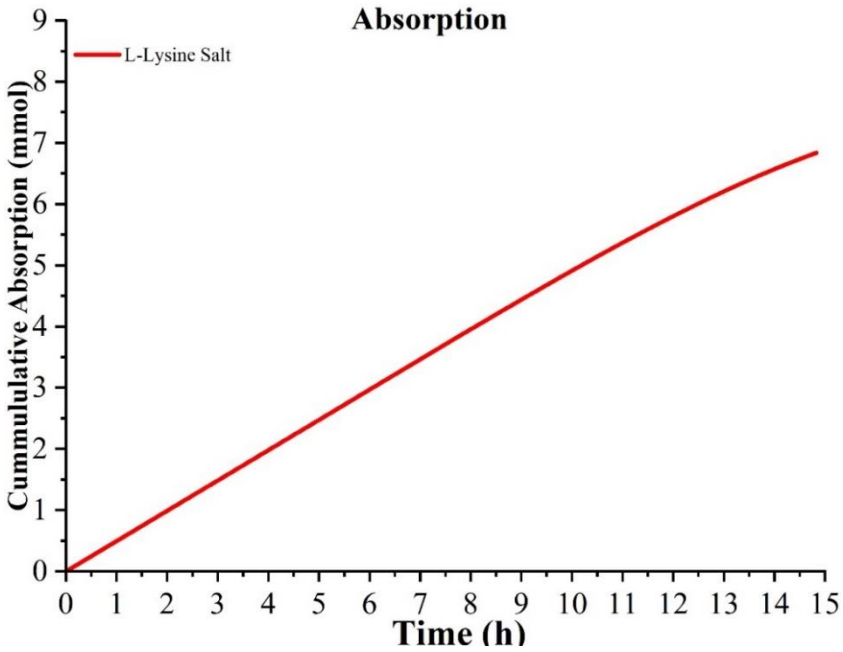

Figure 29. L-Lysine Salt Cumulative Absorption 15 hours.

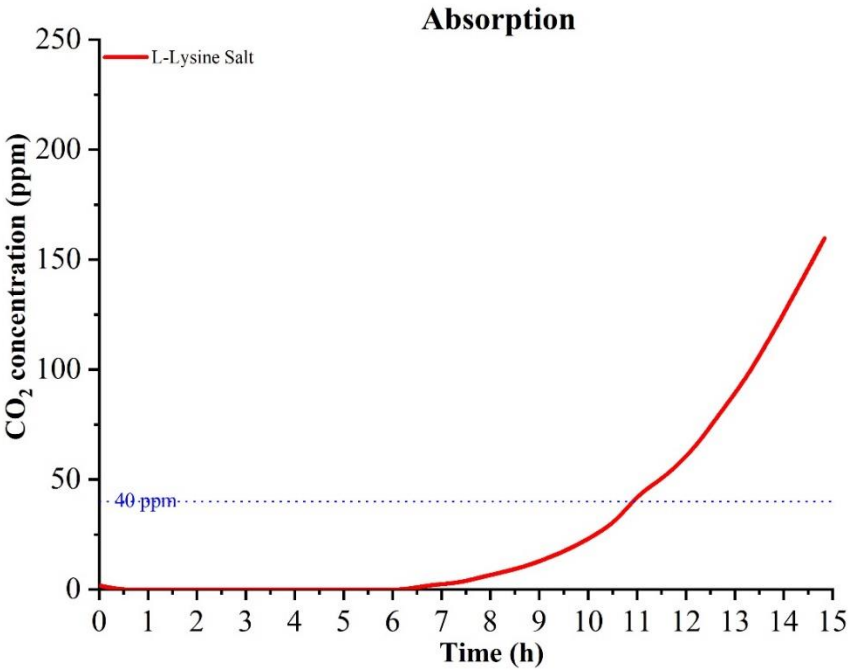

Figure 30. L-Lysine Salt Absorption Concentration 15 hours.

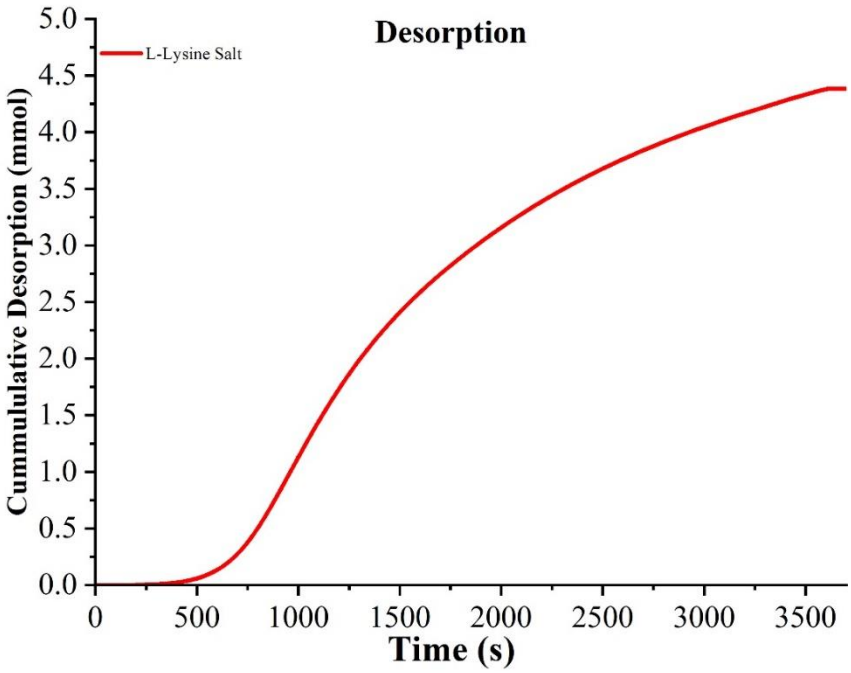

Figure 31. L-Lysine Salt Cumulative Desorption 15 hours.

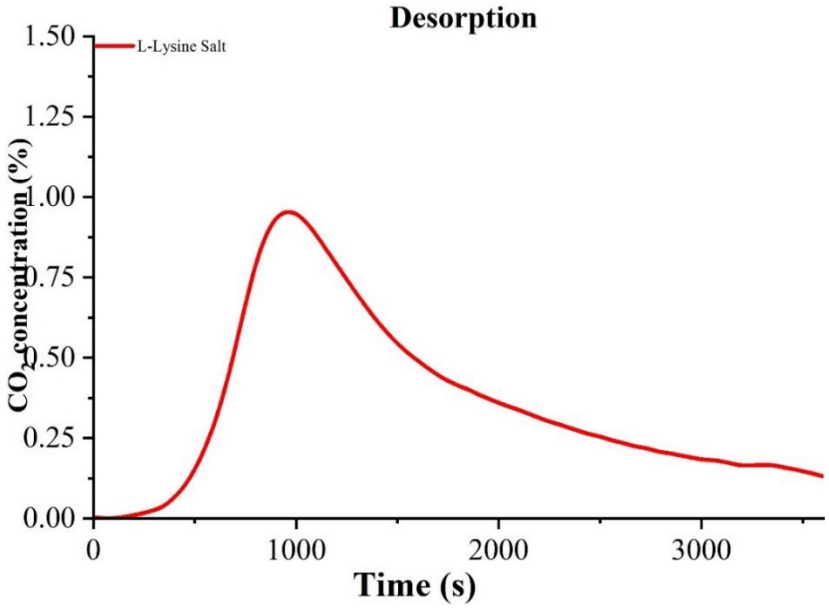

Figure 32. L-Lysine Salt Desorption Concentration 15 hours.

5.3. L-Lysine with 0.01 g (SBA-15, Na-3DG, K-3DG, and Mg-3DG)

Furthering the study of l-lysine as a CO_2 absorbent yielded the following results. The standard l-lysine solution showed a cumulative absorption of 2.188 mmol and

breakthrough time of 0.95 hours, as seen in Figure 33 and Figure 34. However, it is shown that l-lysine with 0.01 g Na-3DG has the highest absorption capacity. The cumulative absorption was 2.223 mmol and the breakthrough time 1.57 hours. This is followed by l-lysine with 0.01 g K-3DG, it has a cumulative absorption amount of 2.207 mmol and breakthrough time of 1.27 hours. L-lysine with 0.01 g Mg-3DG and l-lysine with 0.01 g SBA-15 showed the lowest absorption capacity of 2.192 mmol and 2.182 mmol respectively. Their breakthrough times are also lower than the other catalysts at 1.19 hours for l-lysine with 0.01 g Mg-3DG, and 0.63 hours for l-lysine with 0.01 g SBA-15. All of this is shown in Figure 33 and Figure 34 below.

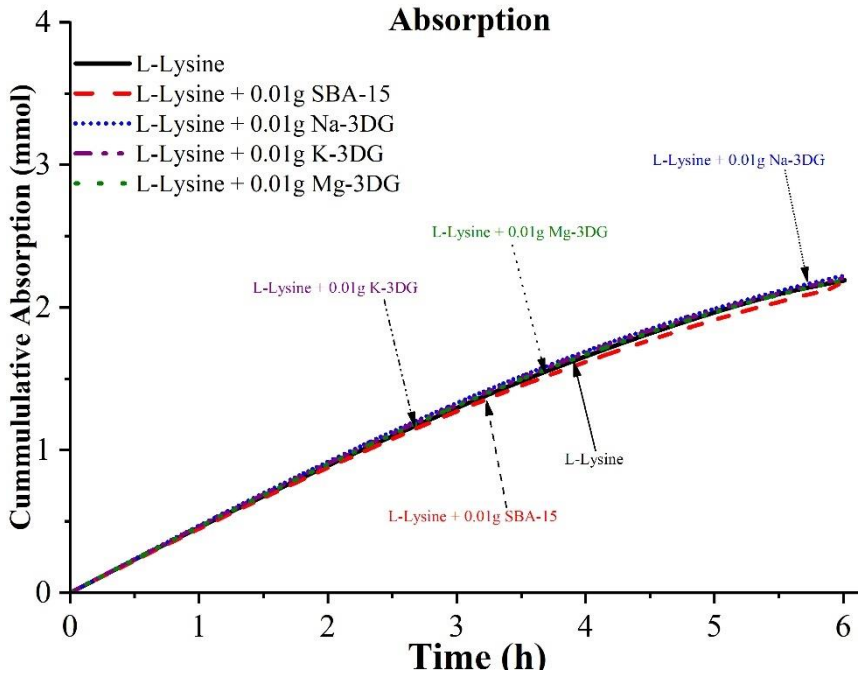

Figure 33. Cumulative Absorption L-Lysine With Different Catalysts.

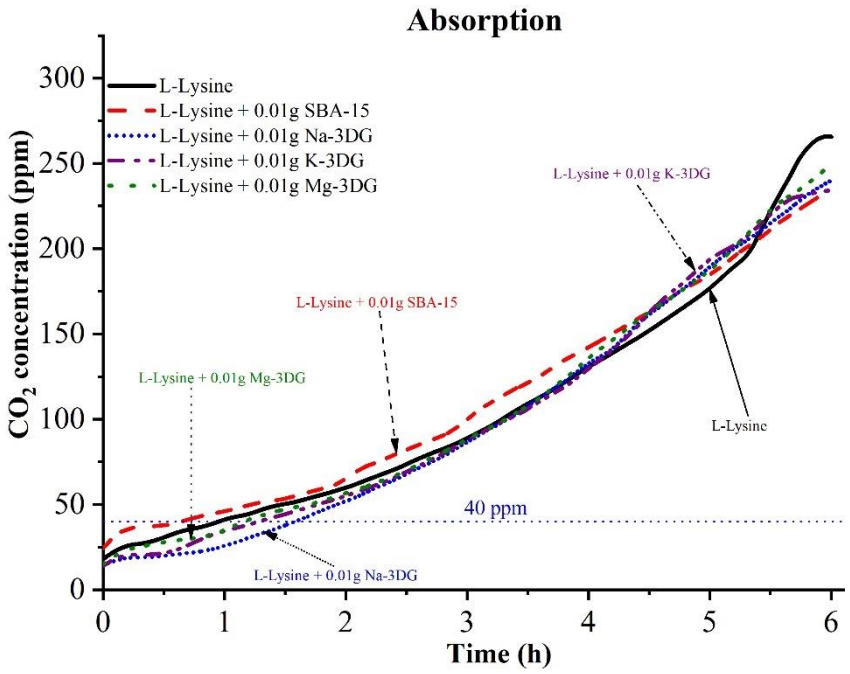

Figure 34. Absorption Concentration L-Lysine With Different Catalysts.

The desorption results follow an expected trend. This part of the experiment was also operated at 95 ºC. The l-lysine and 0.01 g Na-3DG solution has the highest cumulative desorption at 2.616 mmol, this is shown in Figure 35 below. However l-lysine with 0.01 g SBA-15 has the fastest desorption rate, shown in Figure 36. The second highest desorption amount turned out to be the l-lysine solution with 0.01 g Mg-3DG at 2.613 mmol. Followed by the standard l-lysine solution with a cumulative desorption of 2.592 mmol, then l-lysine with 0.01 g K-3DG at 2.548 mmol and finally l-lysine with SBA-15 at 2.425 mmol. The summary of cumulative absorption and desorption is shown in the bar graph Figure 37 below.

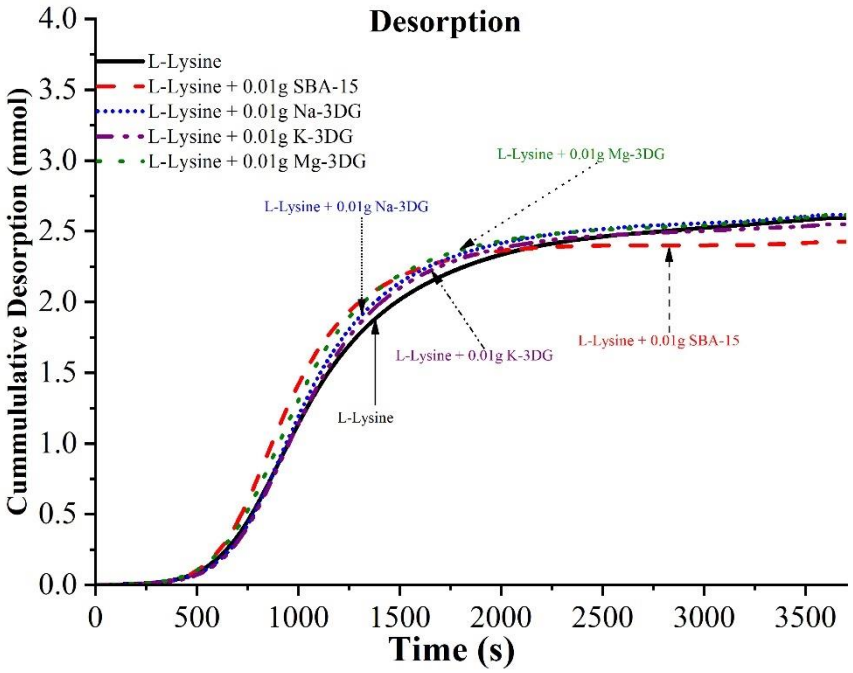

Figure 35. Cumulative Desorption L-Lysine With Different Catalysts.

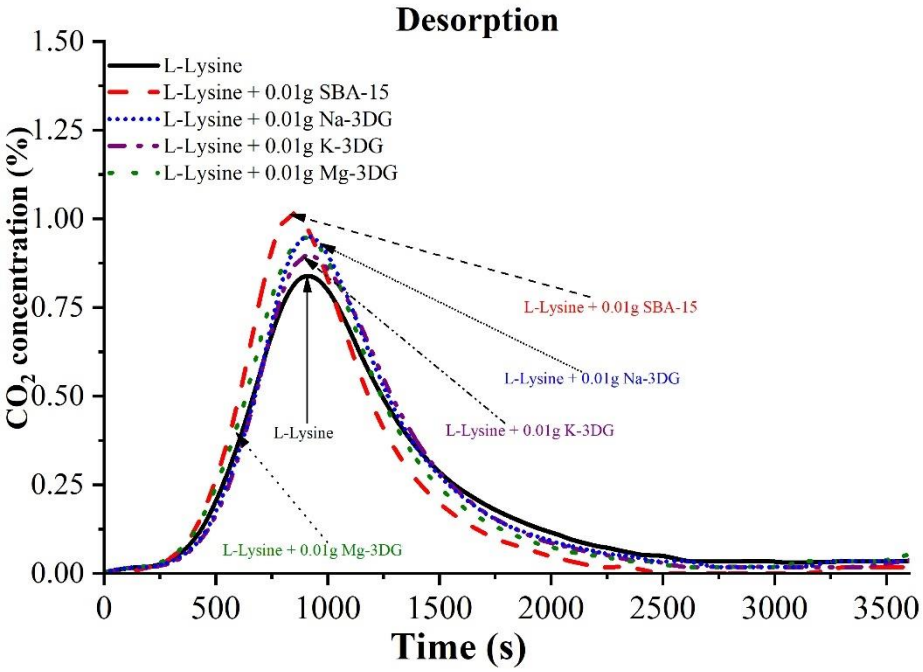

Figure 36. Desorption Concentration L-Lysine With Different Catalysts.

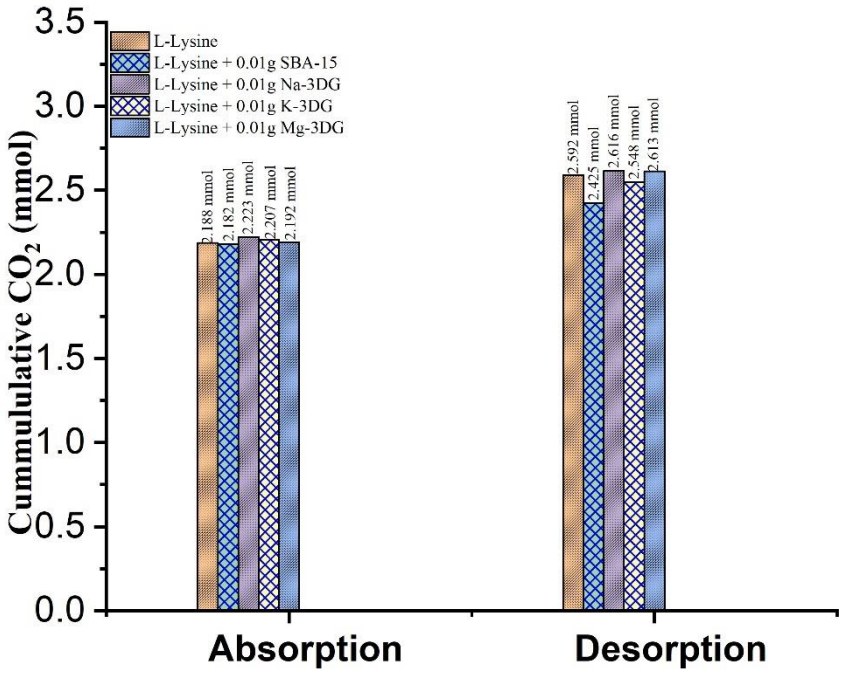

Figure 37. Cumulative Absorption and Desorption Amount L-Lysine With Different Catalysts.

5.4. L-Lysine with 0.005 g, 0.01 g, 0.02 g, and 0.04 g Na-3DG Catalyst

From the experiment with different catalysts, it was concluded that l-lysine with Na-3DG yielded the highest CO_2 absorption and desorption, with the highest breakthrough time. The effect of catalyst is further studied in different quantities. Starting with 0.01 g as seen in the previous section, 0.005 g of Na-3DG was tested, followed by 0.02 g and 0.04 g of Na-3DG.

The desorption step of this experiment was operated at 70 ºC, instead of 95 ºC as done in previous experiments. It was determined that the catalyst improved absorption and the desorption to the extent that the desorption temperature can be lowered. This could reduce the energy requirement for desorption. The result of this study is shown.

The cumulative absorption amount for 0.005 g, 0.01 g, 0.02 g, and 0.04 g Na-3DG are extremely close, at 2.193 mmol, 2.180 mmol, 2.174 mmol, and 2.219 mmol respectively.

It could be said that the use of the catalyst in those amounts does not significantly improve the absorption capacity, but it does improve the breakthrough time. For 0.005 g and 0.01 g Na-3DG, the breakthrough time was 1.36 hours. For the solution with 0.02 g Na-3DG, the breakthrough time was 1.72 hours and finally for 0.04 g Na-3DG the breakthrough time was 1.64 hours. This makes the solution with 0.02 g Na-3DG the preferable one for absorption based on its breakthrough time and cumulative absorption amount. All of this is shown in Figure 38 and Figure 39.

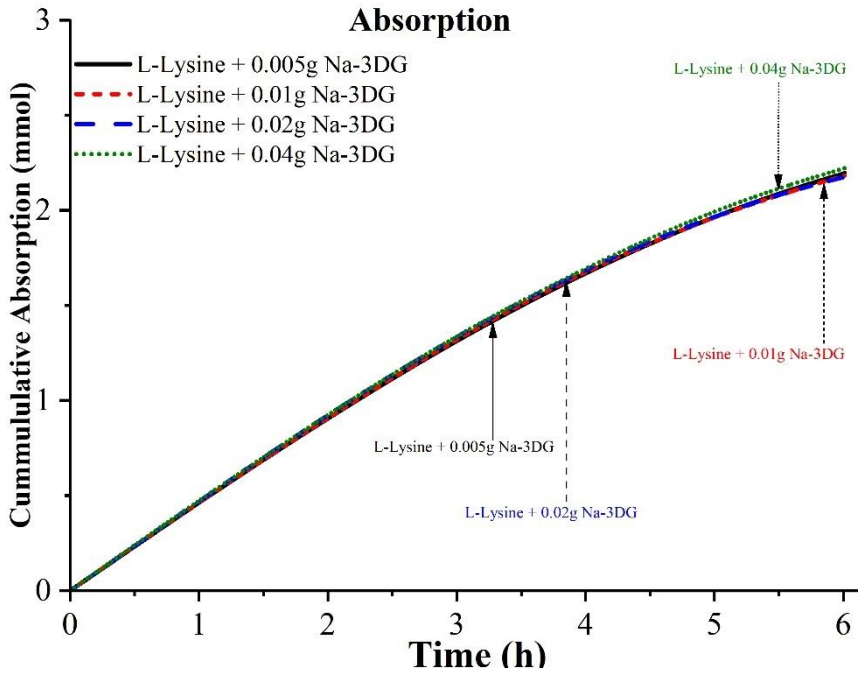

Figure 38. Cumulative Absorption L-Lysine With Varying Na-3DG Ratios.

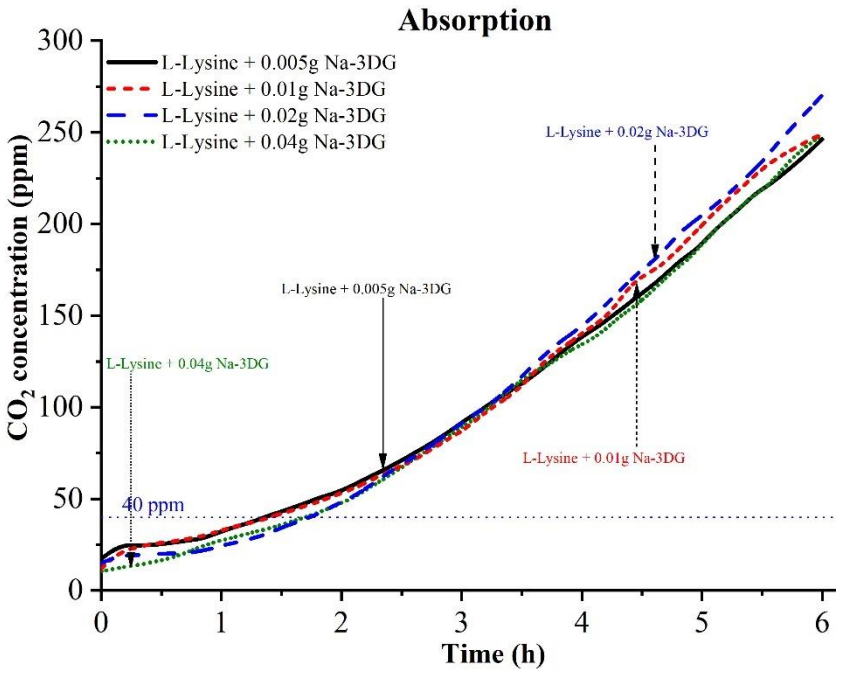

Figure 39. Absorption Concentration L-Lysine With Varying Na-3DG Ratios.

For the desorption experiment carried out at 70 ºC, the cumulative amount of CO_2 desorbed using; 0.05 g Na-3DG was 2.216 mmol, 0.01 g Na-3DG was 2.133 mml, 0.02 g Na-3DG was 2.139 mmol, and 0.04 g Na-3DG was 2.159 mmol. Shown in Figure 40 and Figure 41. As seen during absorption, desorption does not change much with a different amount of catalyst, although taking into account all four results (breakthrough time, absorption capacity, desorption rate, and cumulative desorption), 0.02 g Na-3DG seems to the most ideal. With 0.04 g Na-3DG being a close second and 0.005 g Na-3DG coming in as the third preference. The absorption and desorption amounts are summarized in Figure 42.

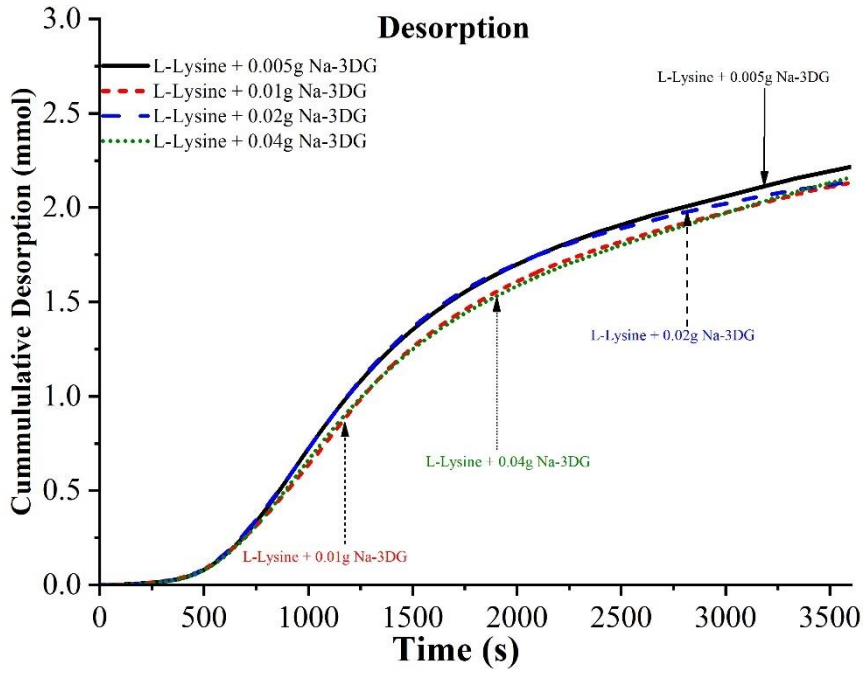

Figure 40. Cumulative Desorption L-Lysine With Varying Na-3DG Ratios.

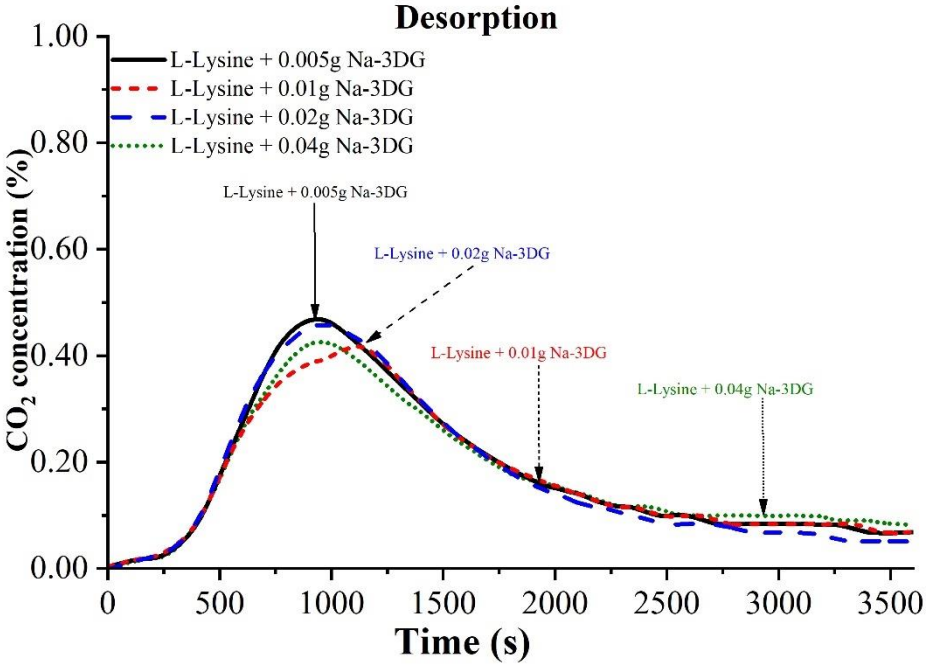

Figure 41. Desorption Concentration L-Lysine With Varying Na-3DG Ratios.

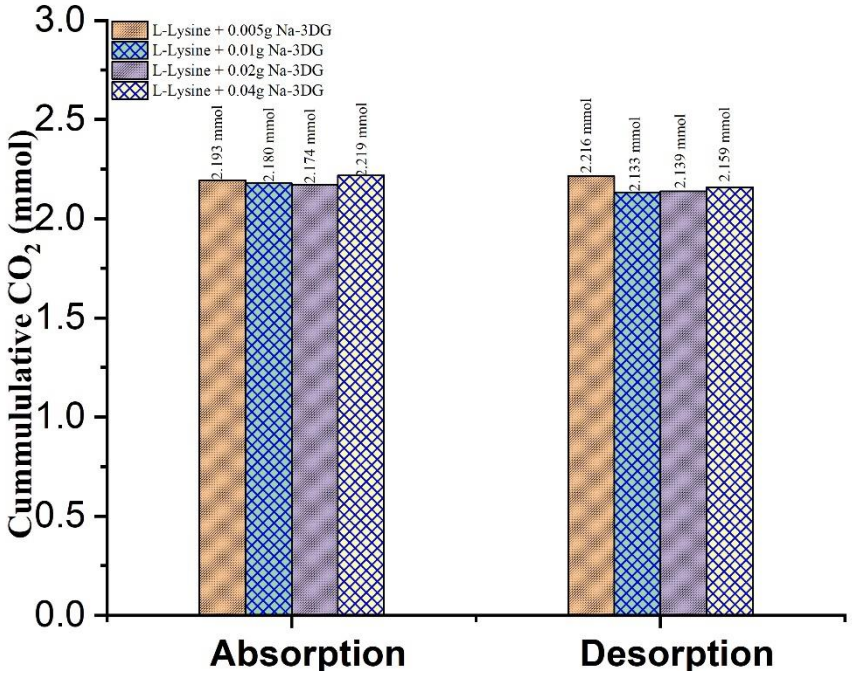

Figure 42. Cumulative Absorption and Desorption Amount L-Lysine With Varying Na-3DG Ratios.

5.5. Multi-Cycle Experiment of L-Lysine with 0.02 g Na-3DG

In order to test the stability of l-lysine with 0.02 g Na-3DG, 11 cycles of experiment was run with one solution/catalyst mixture. The system proved to be stable over time and multiple experiments, with ranges of; 2.169 – 2.253 mmol for cumulative absorption, 2.046 – 2.226 mmol for cumulative desorption, and 1.41 – 1.83 hours for the breakthrough time. All of this is shown in Figure 43, Figure 44, Figure 45, Figure 46, and Figure 47.

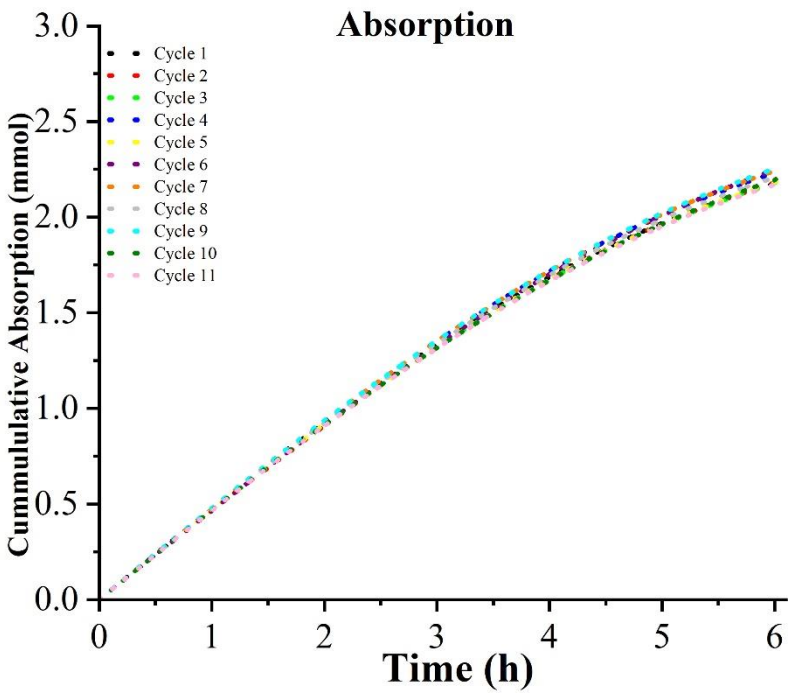

Figure 43. Cumulative Absorption L-Lysine With 0.02g Na-3DG Multicycle.

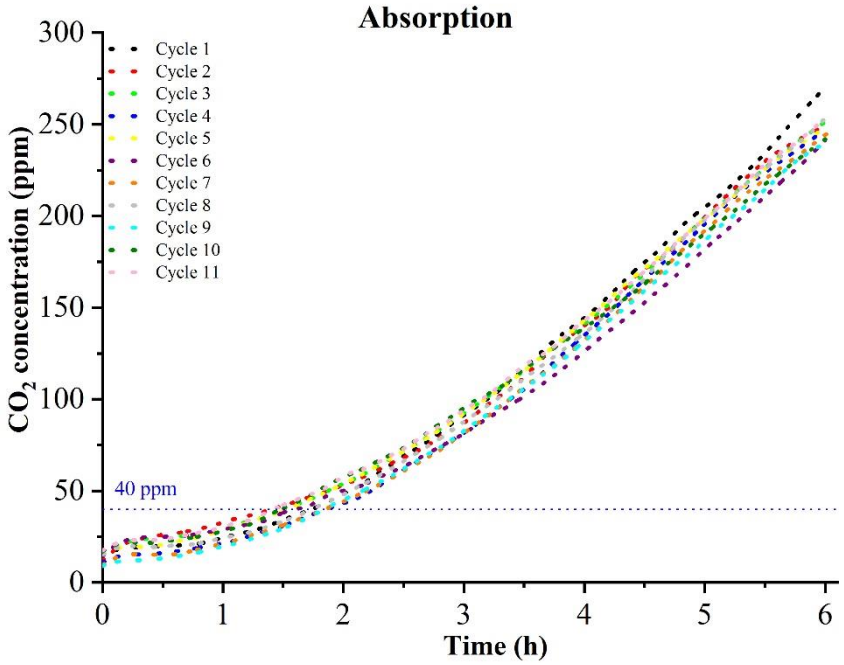

Figure 44. Absorption Concentration L-Lysine With 0.02g Na-3DG Multicycle.

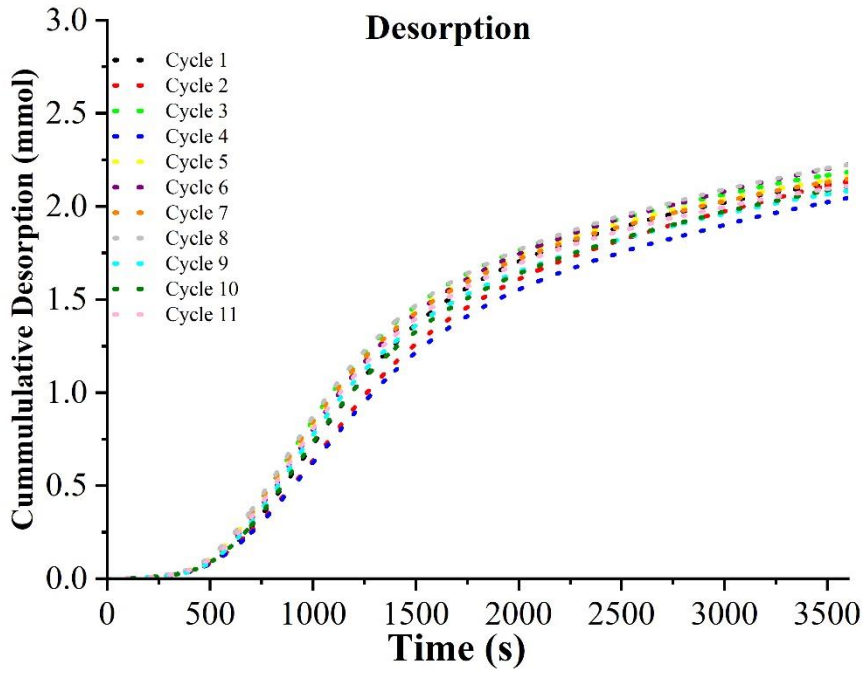

Figure 45. Cumulative Desorption L-Lysine With 0.02g Na-3DG Multicycle.

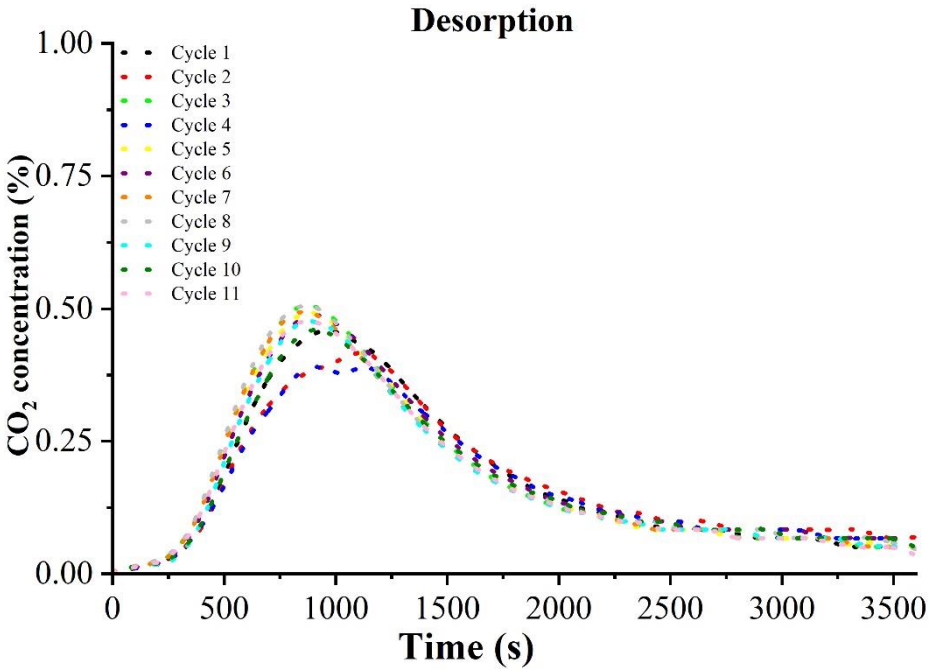

Figure 46. Desorption Concentration L-Lysine With 0.02g Na-3DG Multicycle.

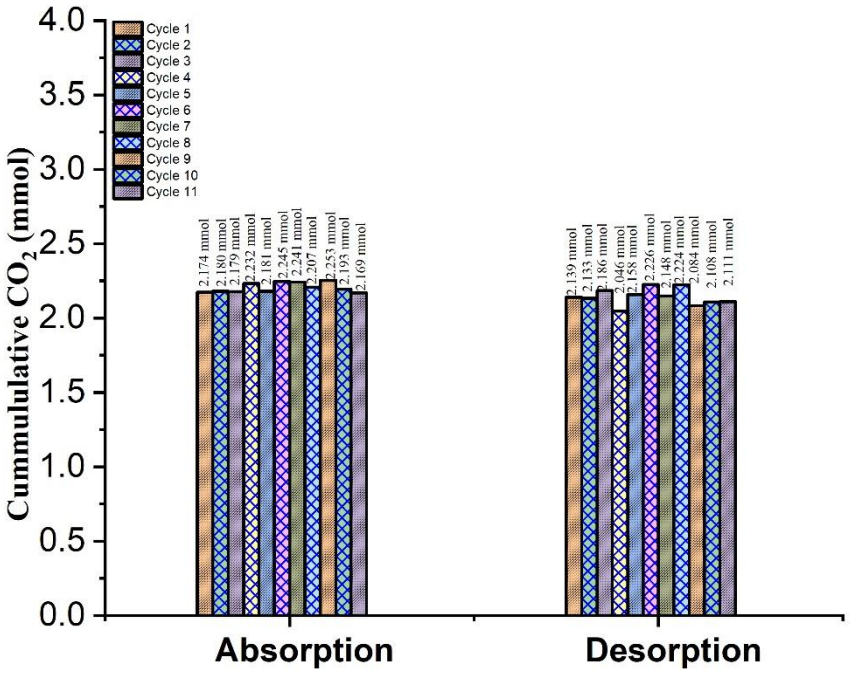

Figure 47. Cumulative Absorption and Desorption Amount L-Lysine With 0.02g Na-3DG Multicycle.

Chapter 6: Discussion

All of the results from Chapter 5 are summarized in this section. From the absorption curves, desorption curves, and bar graphs, we could summarize the cumulative absorption and desorption amounts and the approximate breakthrough time. Table 4 shows a summary of the results from the MEA and amino acids experiments. As previously stated, MEA shows a high absorption capacity, desorption amount and breakthrough time as expected. Followed by l-lysine with the next highest absorption and desorption amounts, and breakthrough time. L-arginine, glycine, and l-histidine had the lowest breakthrough times and cumulative absorption in that order.

Table 4. Summary of MEA Comparison to Amino Acids.

10 mmol Absorbent Solution	Cumulative CO_2 Absorption (mmol)	Cumulative CO_2 Desorption (mmol)	Breakthrough Time (hr.)
MEA	2.768	2.416	3.95
L-Arginine	2.128	1.969	0
L-Histidine	0	0.059	0
L-Lysine	2.188	2.592	0.95
Glycine	0.011	0.037	0

Table 5 shows a summary of the results from the MEA and amino acid salt experiments. MEA shows a high absorption capacity, high desorption and breakthrough time as expected, but l-lysine salt proved to have the highest absorption capacity and breakthrough time (greater than 6 hours). After l-lysine salt, l-arginine salt had the next best absorption capacity and a breakthrough time similar to l-lysine salt (greater than 6 hours), but the cumulative desorption of l-lysine salt and l-arginine salt was the lowest

in the group. Since the experiments only run for 6 hours during absorption and 1 hour during desorption, using l-lysine salt or l-arginine salt for further experimentation in this research was not feasible. More work needs to be done in the exploration of l-lysine salt as an absorbent, preferably running much longer > 12-hour experiments, as it was found that the breakthrough time of l-lysine salt was ~ 11 hours. After l-arginine, MEA had the next best absorption capacity and breakthrough time, followed by glycine salt, and l-histidine salt.

Table 5. Summary of MEA Comparison to Amino Acid Salt.

10 mmol Absorbent Solution	Cumulative CO_2 Absorption (mmol)	Cumulative CO_2 Desorption (mmol)	Breakthrough Time (hr.)
MEA	2.768	2.416	3.95
L-Arginine Salt	2.895	0.085	> 6
L-Histidine Salt	2.277	1.944	2.07
L-Lysine Salt	2.909	1.283	> 6
Glycine Salt	2.715	1.974	3.92
L-Lysine Salt	6.840	4.380	10.85

From the previous groups of tests above, it was determined that l-lysine had the most ideal properties for further study. Its breakthrough time was within the 6-hour range during absorption, and it has a relatively high absorption and desorption capacity. From Table 6, it can be concluded that l-lysine with 0.01 g Na-3DG showed the best absorption, desorption, and breakthrough time. followed by 0.0.1 g K-3DG, 0.01 g Mg-3DG, l-lysine standard solution and 0.01 g SBA-15. Although the solution with 0.01 g Mg-3DG desorbs slightly higher CO_2 than the solution with 0.01 g K-3DG.

Table 6. Summary of L-Lysine With Different Catalysts.

10 mmol Absorbent Solution	Cumulative CO_2 Absorption (mmol)	Cumulative CO_2 Desorption (mmol)	Breakthrough Time (hr.)
L-Lysine	2.188	2.592	0.95
L-Lysine + 0.01g SBA-15	2.182	2.425	0.63
L-Lysine + 0.01g Na-3DG	2.223	2.616	1.57
L-Lysine + 0.01g K-3DG	2.207	2.548	1.27
L-Lysine + 0.01g Mg-3DG	2.192	2.613	1.19

Finally, after choosing the best catalyst (Na-3DG), it was studied with l-lysine at different ratios. From Table 7, it was determined that while taking into account cumulative absorption, desorption, and breakthrough time, l-lysine with 0.02 g Na-3DG was the best ratio for CO_2 capture. Followed by 0.04 g Na-3DG and 0.005 g Na-3DG.

Table 7. Summary of L-Lysine With Different Ratios of Na-3DG Catalyst.

10 mmol Absorbent Solution	Cumulative CO_2 Absorption (mmol)	Cumulative CO_2 Desorption (mmol)	Breakthrough Time (hr.)
L-Lysine	2.188	2.592	0.95
L-Lysine + 0.005g Na-3DG	2.193	2.216	1.36
L-Lysine + 0.01g Na-3DG	2.180	2.133	1.36
L-Lysine + 0.02g Na-3DG	2.174	2.139	1.72
L-Lysine + 0.04g Na-3DG	2.219	2.159	1.64

Further study was done on the l-lysine with 0.02 g Na-3DG mixture to test its stability for future implementation. As seen in Chapter 5.5., the system proved to be relatively stable over time and multiple experiments. The multicycle experiment results fell within 1.89 % (absorption), 4.21 % (desorption), and 12.96 % (breakthrough time) of the average values.

Chapter 7: Conclusion

The results obtained in this work have been discussed in chapters 5 and 6 above. From the results, the high absorption capacity of MEA was proven. It was also shown that amino acids can compete with MEA in terms of absorption, desorption, and breakthrough time, especially with the addition of KOH or a catalyst. The amino acids showed clear improvement in absorption after the addition of KOH, and this agrees with the fact that the absorption capacity of amino acids significantly improves when neutralized by a base like KOH. After comparing the results of all the experiments and discussing them based on cumulative absorption, desorption, and breakthrough time, it was determined that the l-lysine system with 0.02 g Na-3DG was preferred. The stability of the system has also been proven. Although l-lysine salt is also an excellent absorbent, the breakthrough time exceeded the standard reaction time, and the desorption was relatively low. Due to the scope of this research, the absorption reaction time did not exceed 6 hours rendering l-lysine salt unfavorable. However further experimentation with l-lysine salt is recommended.

Highly promising results were derived from the use of amino acid and amino acid salt solution, nevertheless there was only time to focus on one system (l-lysine) for continued study. For future research, l-lysine salt would be recommended for further testing. More experiments can be run over a longer period of time to determine if the CO_2 uptake could be increased, and the concentration of the solution could also be altered to study the changes to breakthrough time, CO_2 absorption, and CO_2 desorption capacity. After this, l-lysine salt could be studied with Na-3DG just like l-lysine, it is

an excellent catalyst for carbon capture, as its micropore area of 650.2 $m^2 \cdot g^{-1}$ makes it a better system than that of K-3DG 209.5 $m^2 \cdot g^{-1}$ and Mg-3DG 0 $m^2 \cdot g^{-1}$. Lower desorption temperatures in order to reduce the energy requirement and possibly increase CO_2 desorption could be further studied. Followed by the investigation of glycine salt and histidine salt with catalysts, as they also have relatively high absorption and desorption amounts.

Bibliography

Andy Bootha, E. d. S., Odd Gunnar Brakstad (2011). "Environmental impacts of amines and their degradation products: Current status and knowledge gaps."

Bian, Y., S. Shen, Y. Zhao and Y.-n. Yang (2016). "Physicochemical Properties of Aqueous Potassium Salts of Basic Amino Acids as Absorbents for CO2 Capture." Journal of Chemical & Engineering Data **61**(7): 2391-2398.

Bruce Alberts, A. J., Julian Lewis, Martin Raff, Keith Roberts, Peter Walter (2002). Molecular Biology of the Cell, 4th edition.

C2ES. "Controlling Industrial Greenhouse Gas Emissions." 2022, from https://www.c2es.org/content/regulating-industrial-sector-carbon-emissions/.

Christopher K. Mathews, K. E. v. H., Kevin G. Ahern (1999).

Ciftja, A., Hartono, A, Svendsen, HF (2013). "Selection of Amine Amino Acids Salt Systems for CO2 Capture." Energy Procedia **37**: 1597-1604.

DOE. "Carbon Capture, Utilization & Storage." 2022, from https://www.energy.gov/carbon-capture-utilization-storage#:~:text=Carbon%20capture%2C%20utilization%20and%20storage,will%20not%20enter%20the%20atmosphere.

EPA. (2022). "Overview of Greenhouse Gases." 2022, from https://www.epa.gov/ghgemissions/overview-greenhouse-gases.

Feron, P. H. M., and Ten Asbroek, N. (2004). "New solvents based on amino-acid salts for CO2 capture from flue gases."

Guo, D., H. Thee, C. Y. Tan, J. Chen, W. Fei, S. E. Kentish, G. W. Stevens and G. d. Silva (2013). "Amino Acids as Carbon Capture Solvents: Chemical Kinetics and Mechanism of the Glycine + CO2 Reaction." Energy & Fuels **27**: 3898-3904.

Hamborg, E. S., J. P. M. Niederer and G. F. Versteeg (2007). "Dissociation Constants and Thermodynamic Properties of Amino Acids Used in CO2 Absorption from (293 to 353) K." Journal of Chemical & Engineering Data **52**(6): 2491-2502.

Hook, R. J. (1997). "An Investigation of Some Sterically Hindered Amines as Potential Carbon Dioxide Scrubbing Compounds." Industrial & Engineering Chemistry Research **36**: 1779-1790.

IEA. (2021). "Direct Air Capture, IEA, Paris." from https://www.iea.org/reports/direct-air-capture.

Jacco van Holst, P. P. P., John P. M. Niederer, Geert F. Versteeg (2006). "CO2 capture from flue gas using amino acid salt solutions."

Krey V., O. M., G. Blanford, T. Bruckner, R. Cooke, K. Fisher-Vanden, H. Haberl, E. Hertwich, E. Kriegler, D. Mueller, S. Paltsev, L. Price, S. Schlömer, D. Ürge-Vorsatz, D. van Vuuren, T. Zwickel (2014). "Climate Change 2014: Mitigation of Climate Change. Contribution of Working Group III to the Fifth Assessment Report of the Intergovernmental Panel on Climate Change." Annex II: Metrics & Methodology.

NASA. (2022). from https://climate.nasa.gov/.

NASA. (2022). "The Effects of Climate Change." 2022, from https://climate.nasa.gov/effects/.

Olajumobi Akeeb, L. W., Weiguo Xie, RichardD avis, Malek Alkasrawi, Sam Toan (2022). "Post-combustion CO2 capture via a variety of temperature ranges and material adsorption process: A review." Journal of Environmental Management **313**.

P. S. Kumar, J. A. H., P. H. M. Feron, and G. F. Versteeg (2003). "Equilibrium Solubility of CO2 in Aqueous Potassium Taurate Solutions: Part 1. Crystallization in Carbon Dioxide Loaded Aqueous Salt Solutions of Amino Acids." Industrial & Engineering Chemistry Research

Paul J. Runci, J. J. D. (2004). "Research and Development Trends for Energy." Encyclopedia of Energy: 443-449.

Quach Nguyen Khanh Nguyen, N. T. Y., Nguyen Duc Hau, Hoai Lam Tran (2020). "Synthesis and Characterization of Mesoporous Silica SBA-15 and ZnO/SBA-15 Photocatalytic Materials from the Ash of Brickyards." Journal of Chemistry **2020**.

Ramezani, R., S. Mazinani and R. D. Felice (2022). "State-of-the-art of CO2 capture with amino acid salt solutions." Reviews in Chemical Engineering **38**(3): 273-299.

Rochelle, G. T. (2009). "Amine Scrubbing for CO2 Capture." Science **325**.

Roongrat Sakwattanapong, A. A., Amornvadee Veawab (2009). "Reaction rate of CO2 in aqueous MEA-AMP solution: Experiment

and modeling." Energy Procedia **1**: 217-224.

Sang Sefidi, V. and P. Luis (2019). "Advanced Amino Acid-Based Technologies for CO2 Capture: A Review." Industrial & Engineering Chemistry Research **58**(44): 20181-20194.

Silva, D. P. B. d. and E. Falck (2005). Computational Chemistry Study of Solvents for Carbon Dioxide Absorption.

Sorensen, M. (2016). Limitations of Carbon Capture and Sequestration. S. University.

Sun, Z. and Y. H. Hu (2021). "3D Graphene Materials from the Reduction of CO2." Accounts of Materials Research **2**(1): 48-58.

WRI. (2022). "Carbon Capture and Storage (CCS)." from https://www.wri.org/initiatives/carbon-capture-and-storage-ccs#:~:text=Carbon%20capture%20and%20storage%20(CCS)%20is%20a%20technological%20process%20that,emissions%20from%20energy%2Dintensive%20industries.